NJC

Accepted Manuscript

Volume 40 | Number 1 | January 2016 | Pages 1–846

NJC
New Journal of Chemistry
www.rsc.org/njc

A journal for new directions in chemistry

ISSN 1144-0546

PAPER
Jason B. Benedict et al
The role of atropisomers on the photo-reactivity and fatigue of diarylethene-based metal–organic frameworks

This is an Accepted Manuscript, which has been through the Royal Society of Chemistry peer review process and has been accepted for publication.

Accepted Manuscripts are published online shortly after acceptance, before technical editing, formatting and proof reading. Using this free service, authors can make their results available to the community, in citable form, before we publish the edited article. We will replace this Accepted Manuscript with the edited and formatted Advance Article as soon as it is available.

You can find more information about Accepted Manuscripts in the author guidelines.

Please note that technical editing may introduce minor changes to the text and/or graphics, which may alter content. The journal's standard Terms & Conditions and the ethical guidelines, outlined in our author and reviewer resource centre, still apply. In no event shall the Royal Society of Chemistry be held responsible for any errors or omissions in this Accepted Manuscript or any consequences arising from the use of any information it contains.

ROYAL SOCIETY OF CHEMISTRY

rsc.li/njc

Syntheses and characterization of monobasic tridentate Cu(II) Schiff-base complexes for efficient oxidation of 3,5-di-*tert*-butylcatechol and oxidative bromination of organic substrates.

Sweta Kumari[a], Arun Kumar Mahato[a], Abhishek Maurya[a], Vijay Kumar Singh[a], Neha Keshwarwani[a], Payal Kachhap[a], Igor Koshevoy[b], Chanchal Haldar[a]*

[a] Department of Applied Chemistry, Indian Institute of Technology (Indian School of Mines), Dhanbad 826004, Jharkhand, India
[b]Department of Chemistry, University of Eastern Finland, Joensuu, 80101, Finland
*To whom correspondence should be addressed. E-mail: chanchal0007@gmail.com
haldar.c.ac@ismdhanbad.ac.in; Fax: +91-326-2235115; Tel: +91-326-2235115

ABSTRACT

Two monomeric copper complexes [Cu^{II}(sal-ppzH)Cl_2] (**1**) and [Cu^{II}(hyap-ppzH)Cl_2] (**2**) were synthesized by reacting $CuCl_2.2H_2O$ with the monobasic tridentate Schiff-base ligands [Hsal-ppz] (**I**) and [Hyap-ppz] (**II**) (derived by reacting 1-(2-Aminoethyl) piperazine with salicylaldehyde and 2-hydroxyacetophenone) respectively. Elemental analysis, IR, UV-Vis, ^{1}H NMR and ^{13}C NMR data confirms the structures of the ligands and that of the complexes. Both complexes are monomeric in nature in solid state and in solution as well. Single crystal XRD data suggests a distorted square pyramidal geometry for **1** and crystallized in $P\bar{1}$ space group. DFT studies established the similar molecular structure for **2**. Synthesized metal complexes [Cu^{II}(sal-ppzH)Cl_2] (**1**) and [Cu^{II}(hyap-ppzH)Cl_2] (**2**) successfully catalyzed the oxidation of 3, 5-di-*tert*-butylcatechol (3,5-DTBC) in methanol in the presence of H_2O_2 with a high K_{cat} value, 1.182×10^4 mmolh^{-1} and 2.880×10^4 mmolh^{-1} respectively. [Cu^{II}(sal-ppzH)Cl_2] (**1**) and [Cu^{II}(hyap-ppzH)Cl_2] (**2**) also anchored into the polymeric matrix of chloromethylated polystyrene and analyzed by TGA, Atomic Absorption Spectroscopy (AAS), EPR, Scanning Electron Micrographs (SEM) as well as Energy Dispersive X-ray (EDX) analysis. Polymer grafted metal complexes were used as catalyst precursors in the oxidative bromination of salicylaldehyde in the presence of H_2O_2,KBr and $HClO_4$.Under optimized reaction conditions, both catalysts show nearly quantitative oxidative bromination of salicylaldehyde with the order of % products formed, 5-bromosalicylaldehyde>3,5-

dibromosalicylaldehyde>3-bromosalicylaldehyde. Plausible reactive species involved in the catalytic cycle are identified by UV-Vis spectroscopic, pH metric titration, ESI-MS, EPR and DFT studies.

1. Introduction

For the development of new metal complexes with novel structure and reactivity, design of the ligand is the most crucial step. In coordination chemistry, schiff-base complexes have been studied extensively. Schiff-base complexes are easy to synthesize, have structural diversities and endless possibilities towards various applications including catalysis.[1-3] Whereas piperazine containing schiff-base complexes are also known for their anthelmintic[4], antimicrobial[5,6] acetyl cholinesterase inhibition[7], melanocortin-4-receptor (MC4-R)[8,9], drug designer[10] anti-PAF[11,12], anti-HIV[13,14] and anti-obesity[15] activities.

Copper containing enzyme, catechol oxidase is responsible for the two electron oxidation of various ortho-diphenols into corresponding ortho-diquinones (shown in the Scheme 1). It was believed that oxidation of polyphenols into corresponding quinones and their polymerization is the major route for melanin formation. In humans, progressive accumulation of melanin or redistribution of epidermal melanin is the main reason for the dark or light patches which may be considered esthetically displeasing.[16,17] In plants polymerization of polyphenols creates enzymatic browning of fruits and vegetables which causes changes in nutritional and organoleptic properties and also diminished storage life and product values.[18] However, oxidation of polyphenols can be beneficial and even considered essential to the quality of a product. Oxidation of polyphenols in processing of black tea, coffee and cocoa enhances their quality, making products richer in flavor and providing unique organoleptic properties.[16,17] Polyphenols oxidation reactions are also of great importance in medical diagnosis for the determination of the hormonally active catecholamines: adrenaline, noradrenaline and l-dopa (l-3, 4-dihydroxyphenylalanine).[19,20] In plants auto polymerization of polyphenols produces melanin. One of the main functions of melanin is to protect the damaged tissues against pathogens and insects.[21]Catechol oxidase enzyme thus provides the disease resistance power in higher plants.
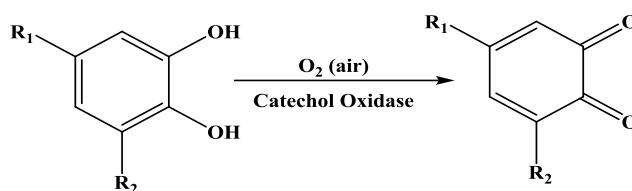
Scheme 1:Oxidation of 3,5-Di-tert-butylcatechol

There are more than 250 structural/functional mimics known for the above enzymes.[22] Inmajorityof the model complexes, the main focus was to mimic the active site coordination environment as close as possible, that lead to the development of various mono nuclear and binuclear metal complexes. Though several binuclear copper complexes successfully emulate the enzyme, both structurally and functionally.[23-26] While few mononuclear copper complexes are also known to exhibit catecholase activity.[27–29] A few non-copper complexes like, Co (II/III)[30-34], Mn (II/III)[35-38], Ni (II)[39-42], Zn (II)[43,44] etc. were also reported as functional models of catechol oxidase and show significant catecholase activity. Besides these, a few Fe[II/III44-49] complexes are also known for their catecholase activity. The main aim of mimicking the active site is to design the molecules that are as efficient as the parent enzyme. But so far none of the reported mono or binuclear Cu(II) complexes reaches the activity that is close to the native enzyme.

Along with the oxidation of polyphenols, oxidative bromination of organic compounds is also one of the important organic transformation in the field of synthesis and industrial applications.[50] Although the classic bromination of organic substrate faces a number of environmental and economical challenges.[51,52] In recent time, using vanadium haloperoxidase model complexes as a catalyst, in presence of KBr and aqueous hydrogen peroxide, is the most green, economical and mild alternative for the oxidative bromination of organic substrates. Vanadium haloperoxidase is a vanadium containing metalloenzyme,[53-58] which primarily oxidizes halides into hypohalous acid in the presence of H_2O_2, and if suitable organic substrate is available then it can halogenate the organic molecules. A number of vanadium oxo-complexes along with some metal phthalocyanines [M = Cu(II), Fe(II) and Co(II)]have been reported as functional models of vanadium haloperoxidase, homogeneously as well as heterogeneously.[59-62]

However, recyclability and separation from reaction mixture are main disadvantages of homogeneous catalysis, which can be overcome by anchoring catalysts in to an insoluble support. Presently Merrifield Resin (Chloromethylated polystyrene cross linked with divinylbenzene) is extensively used for immobilization of homogeneous catalysts. Polymer matrix controls the

activity and selectivity of the catalytic reaction, while giving the advantages of homogeneous as well as heterogeneous catalysts. However, there are few literature reports available regarding the catalytic activity of oxidative bromination of salicylaldehyde by polymer anchored copper complexes.[63-64]

Hence, we have designed two monobasic tridentate ligands (derived by reacting 1-(2-aminoethyl) piperazine with Salicylaldehyde and 2-Hydroxyacetophenone) in such a way that the corresponding copper complexes can provide required steric as well as electronic environment for the oxidation of polyphenols and oxidative bromination of organic substrates. These synthesized mono nuclear copper(II)complexes possess following structural features which may enhance their catalytic activity.

i. Both mono nuclear Cu(II) complexes adopt a distorted square pyramidal geometry. According to literature non-planar geometry is necessary for the catecholase activity.[65]

ii. Reported copper complexes were isolated by reacting CuCl$_2$ with monobasic tridentate ligands. Tridentate ligands allow lower coordination number around the metal centre.

iii. There are two labile -Cl groups, which can be easily removed and allow the easy association of substrate molecule with the metal complex.

Although similar ligand systems are known,[66-68] but for the first time we are reporting here the copper complexes of the ligands [Hsal-ppz] (**I**) and [Hyap-ppz] (**II**)with bi-functional catalytic activity towards the oxidation of 3,5-DTBC and oxidative bromination of salicylaldehyde, along with the single crystal XRD data of [Cu^{II}(sal-ppzH)Cl$_2$] (**1**).

2. *Experimental*

2.1. *Chemicals and materials*

All chemicals were obtained from commercial sources and used as received. Analytical grade reagent salicylaldehyde (Lobachemie, India), 2-hydroxyacetophenone (Lobachemie, India), 30 % aqueous H$_2$O$_2$(TCI, Japan),3,5-di-*tert*-butylcatechol (TCI, Japan), CuCl$_2$.2H$_2$O (Lobachemie, India), 70% Perchloric acid (Merck, India), KBr (Merck, India),5-bromosalicylaldehyde (TCI, Japan),3,5-dibromosalicylaldehyde (TCI, Japan),2,4,6-tribromophenol (TCI, Japan), and 1-(2-Aminoethyl)piperazine (Sigma Aldrich, USA) were used as obtained without further purification. All other chemicals and solvents were of analytical reagent grade and used without further purification.

2.2. Instrumentation and Characterization Procedures

Infra-Red spectra of ligands were recorded in solid states as a KBr pellet /ATR mode on a Thermo-NICOLET 8700 Research Spectrometer /Carry 660FTIR spectrometer within the range of 400–4000 cm^{-1}.Electronic spectra were recorded in methanol/nujol with a Shimadzu UV-1800 UV-Vis spectrophotometer. ^{1}H and ^{13}C NMR spectra of the ligands were recorded on a Bruker Avance II 400 MHz NMR spectrometer with the common parameter settings in DMSO-d_6 solvent. Cyclic Voltammograms (CVs) were recorded using a conventional three electrode arrangement using CHI 660C electrochemical analyzer. Thermo gravimetric analyses were performed using NETZSCH-Gerätebau GmbH, STA 449 F3Jupiter instrument, SEM and Energy Dispersive X-ray analyses (EDX)were done by using HITACHI S-3400N, Atomic Absorption Spectroscopic analyses were carried out in LABINDIA AA8000. EPR spectra of the metal complexes were recorded in DMSO on a Bruker EMX X-band spectrometer operating at 100-kHz field modulation at room temperature. For polymer anchored metal complexes spectra were recorded on a Jeol JES-X3 Series ESR spectrometer at 77K. The ESI^{+} mass of the metal complexes were estimated on Waters Q-Tof Micromass instrument. Anagilent 7890 B gas-chromatograph fitted with a HP-5 capillary column (30 m × 0.25 mm × 0.25 i.d.) and a FID detector was used to analyze the reaction products and % conversions were calculated on the basis of the relative peak area of the respective products with the reactant. Identity of the products were confirmed by using commercially available standards and GC-MS (thermo ISQ QD single quadrupole mass analyzer coupled with Trace 1300 GC system).

2.3. X-ray crystallography

The crystal of $[Cu^{II}(sal-ppzH)Cl_2]$ (**1**) was immersed in cryo-oil, mounted in a Nylon loop, and measured at a temperature of 150 K. The diffraction data was collected with Bruker Kappa APEX II diffractometer using Mo Kα radiation (λ = 0.71073 Å). The APEX2[69] program package was used for cell refinements and data reductions. The structures were solved by direct methods using the SHELXS-2014[70] program with the WinGX[71] graphical user interface. A semi empirical absorption correction (SADABS)[72] was applied to all data. Structural refinements were carried out using SHELXL-2014.[71]

Some of the crystallization solvent was lost from the crystal and could not be resolved unambiguously. The contribution of the missing solvent to the calculated structure factors was

taken into account by using a SQUEEZE routine of PLATON.[73] The missing solvent was not taken into account in the unit cell content.

The NH_2 hydrogen atoms were located from the difference Fourier map and constrained to ride on their parent atom, with U_{iso} = 1.2 U_{eq} (parent atom). All other hydrogen atoms in [Cu^{II}(sal-ppzH)Cl_2] (**1**) were positioned geometrically, with C–H = 0.95–0.99 Å, O–H = 0.84 Å, U_{iso} = 1.2 U_{eq} (parent atom). CCDC No. 1539445contain the supplementary crystallographic data for this paper. These data can be obtained free of charge from the Cambridge Crystallographic Data Centre via www.ccdc.cam.ac.uk/data_request/cif. The crystallographic details are summarized in table 1.

Table 1:Crystal data and structure refinement for [Cu^{II}(sal-ppzH)Cl_2] (**1**)

Identification code	1
Empirical formula	$C_{13}H_{19}Cl_2CuN_3O$
Formula weight	367.75
Temperature	150(2) K
Wavelength	0.71073 Å
Crystal system	Triclinic
Space group	$P\bar{1}$
Unit cell dimensions	a = 11.8119(4) Å
	b = 13.0851(4) Å
	c = 13.4912(4) Å
	α = 90.401(1)°
	β = 91.035(1)°
	γ = 107.506(2)°
Volume	1988.13(11) Å^3
Z	4
Density (calculated)	1.229 Mg/m^3
Absorption coefficient	1.366 mm^{-1}
F(000)	756
Crystal size	0.721 x 0.688 x 0.278mm^3
θ range for data	2.039 to 34.679°

collection	
Index ranges	18<=h<=16, -20<=k<=20, -20<=l<=20
Reflections collected	44563
Independent reflections	14061 [R(int) = 0.0204]
Completeness to θ= 25.242°	97.8 %
Absorption correction	Numerical
Max. and min. transmission	0.703 and 0.439
Refinement method	Full-matrix least-squares on F^2
Data / restraints / parameters	14061 / 0 / 361
Goodness-of-fit on F^2	1.031
Final R indices [I>2sigma(I)][a]	R1 = 0.0327, wR2 = 0.0778
R indices (all data)	R1 = 0.0497, wR2 = 0.0839
Largest diff. peak and hole	0.528 and -0.500e.Å^{-3}

[a] $R1 = \Sigma||F_o| - |F_c||/\Sigma|F_o|$; $wR2 = [\Sigma[w(F_o^2 - F_c^2)^2]/ \Sigma[w(F_o^2)^2]]^{1/2}$.

2.4. Computational methods

Density functional theory was used to explore the structural and chemical properties for the synthesized metal complexes**1** and **2**. All the calculations were performed using Gaussian '09[74] program package with the Gauss View 5.0 and Chemcraft[75-76] molecular visualization program using a HP workstation Z440. X-ray refinement data of the mononuclear [Cu^{II}(sal-ppzH)Cl$_2$] (**1**) was taken as an initial guess for the liquid phase geometry optimization. The molecular structure of the compounds in the ground state is optimized by Density Functional Theory (DFT) in its unrestricted forms, employing the LANL2DZ with an effective core potential for Cu atom and 6-

311G (d,p) for the rest of the atoms in methanol using a conductor-like polarizable continuum model (CPCM). In DFT calculation electron correlations were included using Becke3–Lee–Yang–Parr (B3LYP) procedure.[77–79] This includes Becke's gradient exchange corrections, Lee, Yang and Parr correlation functional.[80] Frequency calculation at the same level of theory was performed to ensure that the equilibrium system represents true minima on the potential energy surface. No symmetry constrain was imposed during the geometry optimization.

2.5. Catalytic activity

2.5.1. Oxidation of 3,5-di-tert-butycatechol (catecholase like activity?)

1 and **2** were tested against the catalytic oxidation of 3,5-di-tert-butylcatechol (3,5-DTBC). 3,5-DTBC was chosen because the *tert*-butyl substituent on the ring makes it highly stable and a low quinone–catechol reduction potential makes it easily oxidizable to the corresponding *o*-quinone. In a typical reaction, 1.0×10^{-4} M [Cu^{II}(hyap-ppzH)Cl_2] (**2**) was reacted with 2.85×10^{-2} M 3,5-DTBC and 1.0×10^{-1} M H_2O_2 in a total 20 ml methanolic reaction mixture at room temperature and pressure. Reaction progress was monitored spectrophotometrically for 70 minutes (figure 1). With the course of time, a new absorption band at 400 nm arises. It is well established that 3,5-DTBQ shows characteristic band maxima at 400 nm in methanol which proves catalytic oxidation of 3,5-DTBC. Figure1 shows the spectral changes during the catalytic oxidation of 3,5-DTBC by taking catalyst **2** as a representative. In the absence of catalyst, no conversion was observed. We have observed that the oxidative conversion of 3,5-DTBC is silent in presence of aerial oxygen as well as H_2O_2 individually. To verify the effect of aerial O_2, on the oxidation of 3,5-DTBC, 2.85×10^{-2} M 3,5-DTBC was reacted with 1.0×10^{-4} M of catalyst **2** with and without 1×10^{-1} M H_2O_2 under nitrogen atmosphere separately (plot S2). Plot S2 clearly indicates that, H_2O_2 is necessary for the oxidation of 3,5-DTBC and eliminates any effect of aerial O_2 during oxidation of 3,5-DTBC.
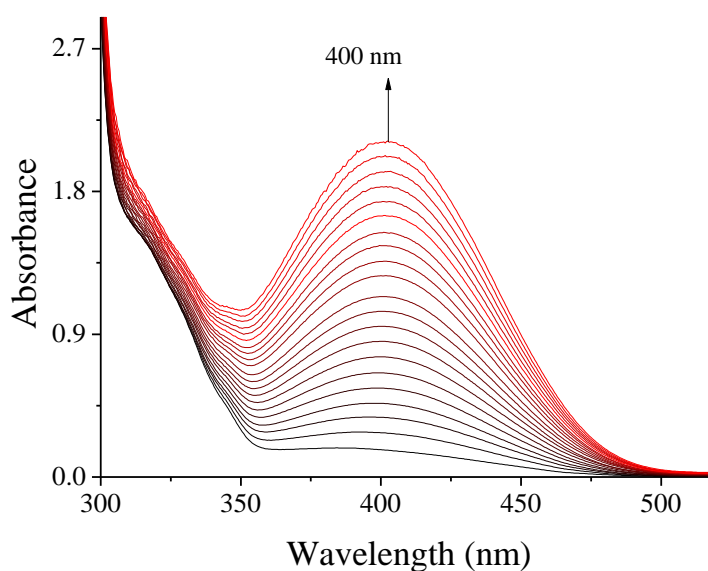
Figure 1: Spectral changes observed during oxidation of 3,5-DTBC (2.85×10^{-2} M) to corresponding *o*-quinone in the presence of 1.0×10^{-1} M H_2O_2 by **2** (1.0×10^{-4} M) in a total 20 ml methanolic reaction mixture at room temperature.

2.5.1.1. Kinetics of catalytic oxidation of 3,5-di-tert-butycatechol

The kinetics of the catalytic oxidation of 3,5-DTBC to corresponding *o*-quinone in the presence of catalysts was monitored by observing the change in absorbance at λ_{max} 400 nm. All the catalysts follow Michaelis-Menten equation of saturated kinetics. To check the catalytic efficiency we have calculated their rate and k_{cat} (i.e. turn over number) by an initial rate method. Plot 1 shows the change in absorbance with time at λ_{max} 400 nm for the conversion of 3,5-DTBC to 3,5-DTBQ with catalyst and without catalyst in the presence of dilute H_2O_2 in methanol for 10 min at room temperature. Multicolored graph in plot 1 shows the effect of various increasing concentrations (1×10^{-1} M, 1×10^{-2} M, 2×10^{-2} M, 4×10^{-2} M, 6×10^{-2} M and 8×10^{-2} M) of 3,5-DTBC on the catalytic oxidation reaction by 1×10^{-4} M methanolic solution of **2** in presence of 1×10^{-1} M H_2O_2 in methanol.

New Journal of Chemistry Accepted Manuscript
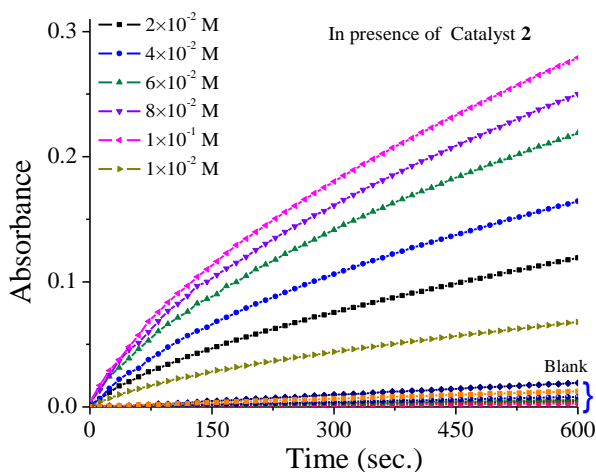
Plot 1: Absorbance vs. time plots for the oxidation of 3,5-DTBC (1×10^{-1} M, 1×10^{-2} M, 2×10^{-2} M, 4×10^{-2} M, 6×10^{-2} M and 8×10^{-2} M) with and without catalyst **2**(1×10^{-4} M) for 10 minutes in the presence of 1.0×10^{-1} M dilute H_2O_2 in methanol at room temperature. (Reaction conditions: 1 ml substrate (1×10^{-1} M, 1×10^{-2} M, 2×10^{-2} M, 4×10^{-2} M, 6×10^{-2} M, 8×10^{-2} M) was reacted with 1 ml H_2O_2 (1×10^{-1} M) and 0.5 ml catalyst (1×10^{-4} M) in presence of 1 ml MeOH.)

2.5.2. *Oxidative Bromination of Salicylaldehyde*

Polymer anchored metal complexes PS-[Cu^{II}(sal-ppz)Cl] (**3**) and PS-[Cu^{II}(hyap-ppz)Cl] (**4**) were used as a catalyst in the oxidative bromination of salicylaldehyde. Salicylaldehyde (1.22g, 10 mmol), 30% aqueous H_2O_2 (2.27 g, 20 mmol), and an aqueous KBr (2.38 g, 20 mmol) solution (20 ml) were mixed in a 100 ml round bottom flask. To this, catalyst ([Cu^{II}(sal-ppz)Cl], (0.010 g) and aqueous 70% HClO$_4$(2.86 g, 20 mmol) (*Caution: HClO$_4$ is strong oxidant, must be handled with care.)* were mixed and kept on stirring for 2 hours at room temperature. For the improvement of catalytic reaction, half of the perchloric acid was added initially (time=0) and rest amount was divided in three equal portions and added after every 15 minutes. Each polymer anchored metal complex was swelled for 6 hours in water before using in catalytic reaction. All the reaction conditions were kept as identical as possible, namely: RPM (800), shape and size of RBF (100 ml) and magnetic stir bar. After 2 hours of reaction, orange colored organic product was extracted with CH$_2$Cl$_2$ and used in GC for the analysis. The formation of three bromo derivatives (5-bromosalicylaldehyde,3,5-dibromosalicylaldehyde and 3-bromosalicylaldehyde) of salicylaldehyde were confirmed by matching the retention time with their commercially available

standards. A single quadrupole GC-MS was also employed to confirm the identity of bromination products of salicylaldehyde.

2.6. Synthesis

2.6.1. Preparation of [Hsal-ppz] (**I**) and [Hyap-ppz] (**II**)

The Schiff-base ligand [Hsal-ppz] (**I**) was prepared by the 1:1 condensation of salicylaldehyde (0.61 g, 5 mmol) and 1-(2-Aminoethyl)-piperazine (0.646 g, 5 mmol) in 30 ml methanol following uninterruptible stirring. The color of the reaction mixture appears yellow and was further refluxed for 2-3 hours. The progress of the reaction was monitored by TLC at regular time intervals. The volume of the reaction mixture was reduced to ~10 ml and kept for 2-3 days at room temperature till the yellow colored solid of [Hsal-ppz] (**I**) separated out. It was filtered, washed with methanol (2×5 ml) followed by petroleum ether and dried over silica gel under vacuum.

Yield: 2.27g (97.39%); Anal. Calcd. for $C_{13}H_{19}N_3O$ (MW: 233.31): C, 66.92 %; H, 8.86 %; N, 18.01 %; Found: C, 67.15 %; H, 8.99 %; N, 17.95 %; FTIR (KBr plate method, cm^{-1})): 3369(ν_{OH}), 2928(ν_{N-H}), 1635($\nu_{C=N}$), 1279(ν_{C-O}); UV-Vis(in MeOH, λ_{max}(nm)/ε(litre mol^{-1}cm^{-1})): 254(1.114×10^4),272(5.726×10^3), 316(3.609×10^3), 405(1.460×10^3); ^{1}H NMR(CDCl$_3$, δ in ppm): 13.27(s, 1H), 4.98(s, 1H), 8.26(s, 1H), 6.78(t, 1H), 6.88(d, 1H), 7.15(d, 1H), 7.22(t, 1H), 2.46(sb, 4H), 2.55(t, 2H), 2.63(m, 2H), 2.93(t, 2H), 3.65(q, 2H).

By adopting the similar procedure as described for the synthesis of ligand [Hsal-ppz] (**I**), we also prepared [Hyap-ppz] (**II**) by reacting 1-(2-Aminoethyl)piperazine with 2-hydroxyacetophenone in methanol.

Data for the ligand [Hyap-ppz] (**II**)

Yield: 2.40 g (97.17 %),Anal. Calcd. For $C_{14}H_{21}N_3O$ (MW: 247.34): C, 67.98%; H, 8.56%; N, 16.99%. Found: C, 68.05%; H, 8.69%; N, 16.84%; FTIR (KBr plate method,cm^{-1}): 3432(ν_{OH}), 2929(ν_{N-H}), 1615($\nu_{C=N}$), 1299(ν_{C-O}); UV-Vis(in MeOH, λ_{max}(nm)/ε(litre mol^{-1}cm^{-1})): 270(7.5138×10^3),324(1.936×10^3), 388(3.508×10^3);^{1}H NMR(CDCl$_3$, δ in ppm):16.20(s, 1H), 5.87(s, 1H), 6.68(t, 1H), 6.85(d, 1H), 7.19(t, 1H), 7.43(d, 1H), 2.45(sb, 4H), 2.68(t, 2H), 2.84(sb, 4H), 3.61(t, 2H), 2.26(s, 3H).

2.6.2.Synthesis of [Cu^{II}(sal-ppzH)Cl$_2$] (**1**) and [Cu^{II}(hyap-ppzH)Cl$_2$] (**2**)

A methanolic solution (20 ml) of [Hsal-ppz] (**I**) (2.31 g, 10 mmol) was added to a methanolic (10 ml) solution of $CuCl_2.2H_2O$ (1.70g, 10 mmol) with constant stirring. After refluxing the reaction mixture for 2 hours, a green colored $[Cu^{II}(sal\text{-}ppzH)Cl_2]$ (**1**) compound separated out. The product was filtered, washed several times with methanol(3×20 ml) and finally dried over silica gel under vacuum.

Data for the complex $[Cu^{II}(sal\text{-}ppzH)Cl_2]$ (**1**)

Yield: 2.82 g (76.85 %); Anal. Calcd. For $C_{13}H_{19}N_3OCl_2Cu$ (MW:367.76): C, 42.46 %; H, 5.21 %; N, 11.43 %;Found: C, 42.60 %; H, 5.33 %; N, 11.32 %;FTIR (ATR mode, cm^{-1}): 3435(ν_{OH}), 2945($\nu_{N\text{-}H}$), 1600($\nu_{C=N}$), 1201($\nu_{C\text{-}O}$); UV-Vis(in MeOH, λ_{max}(nm)/ε(litre mol^{-1}cm^{-1})): 225(2.170×10^3), 238(2.126×10^3), 272(1.8953×10^3), 364(5.194×10^2), 667(88).

Similarly, $[Cu^{II}(hyap\text{-}ppzH)Cl_2]$ (**2**) was isolated by reacting $CuCl_2.2H_2O$ with ligand [Hyap-ppz] (**II**) from refluxing methanol. Scheme 2 represents the probable structure for the synthesized copper (II) complexes.

Data for the complex $[Cu^{II}(hyap\text{-}ppzH)Cl_2]$ (**2**)

Yield: 2.86g (75.19%); Anal.Calcd. For $C_{14}H_{21}N_3OCl_2Cu$ (MW: 381.79): C, 44.04 %; H, 5.54 %; N, 11.01 %; Found: C, 44.19 %; H, 5.62 %; N, 10.98 %; FTIR (ATR mode, cm^{-1}): 3413 (ν_{OH}), 2926($\nu_{N\text{-}H}$),1601($\nu_{C=N}$), 1233($\nu_{C\text{-}O}$); UV-Vis(in MeOH, λ_{max}(nm)/ε(litre mol^{-1}cm^{-1})): 225(2.237×10^3), 270 (1.446×10^3), 354(4.443×10^2), 638(67).
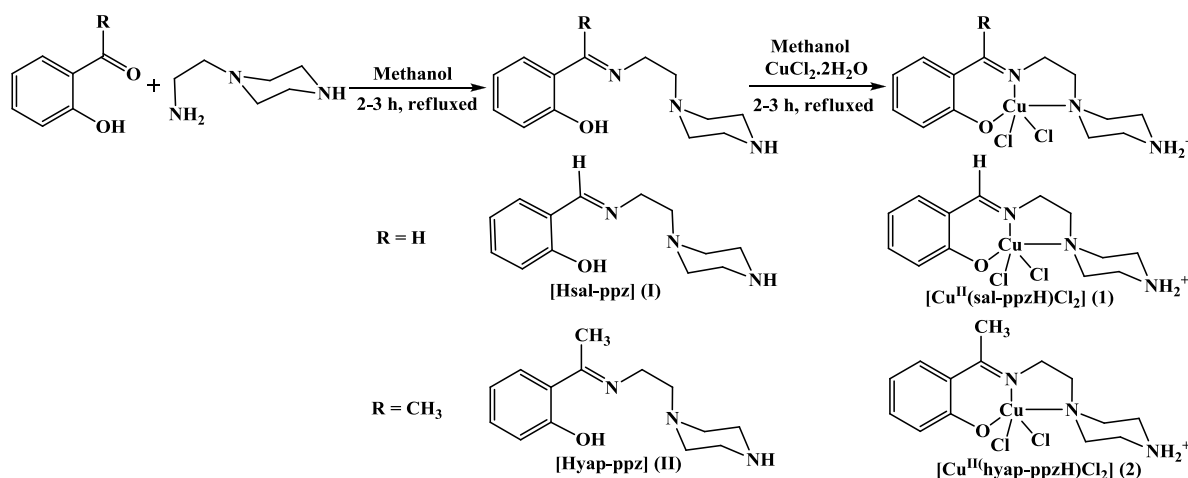

Scheme 2: Synthetic routes and structures for the synthesized ligands and copper(II) complexes.

2.6.3. A general method for the preparation of PS-[Cu^{II}(sal-ppz)Cl] (**3**) and PS-[Cu^{II}(hyap-ppz)Cl] (**4**)

Chloromethylated polystyrene (1.0 g) was allowed to swell in DMF (20 ml) for 6 hours. A solution of [Cu^{II}(sal-ppzH)Cl$_2$] (**1**) (1.838 g, 5 mmol), dissolved in DMF (40 ml) was added to the above suspension. KI (0.830 g, 5 mmol) and triethylamine (3 ml) was added into the reaction mixture with smooth stirring. The whole reaction mixture was refluxed for 48 hours in an oil bath fitted with a water cooled condenser. After the completion of reaction brown colored polymer anchored metal complex was filtered and washed thoroughly with hot DMF (5×20 ml) followed by hot methanol (5×20ml). The isolated polymer anchored metal complex PS-[Cu^{II}(sal-ppz)Cl] (**3**) was dried in hot air oven at *ca.*110 °C for 24 hours. Recovery yield: ~92%.

Similarly PS-[Cu^{II}(hyap-ppz)Cl] (**4**) was prepared by using [Cu^{II}(hyap-ppzH)Cl$_2$] (**2**) (1.908 g, 5 mmol) in place of [Cu^{II}(sal-ppzH)Cl$_2$] (**1**). Recovery yield: 95 %.
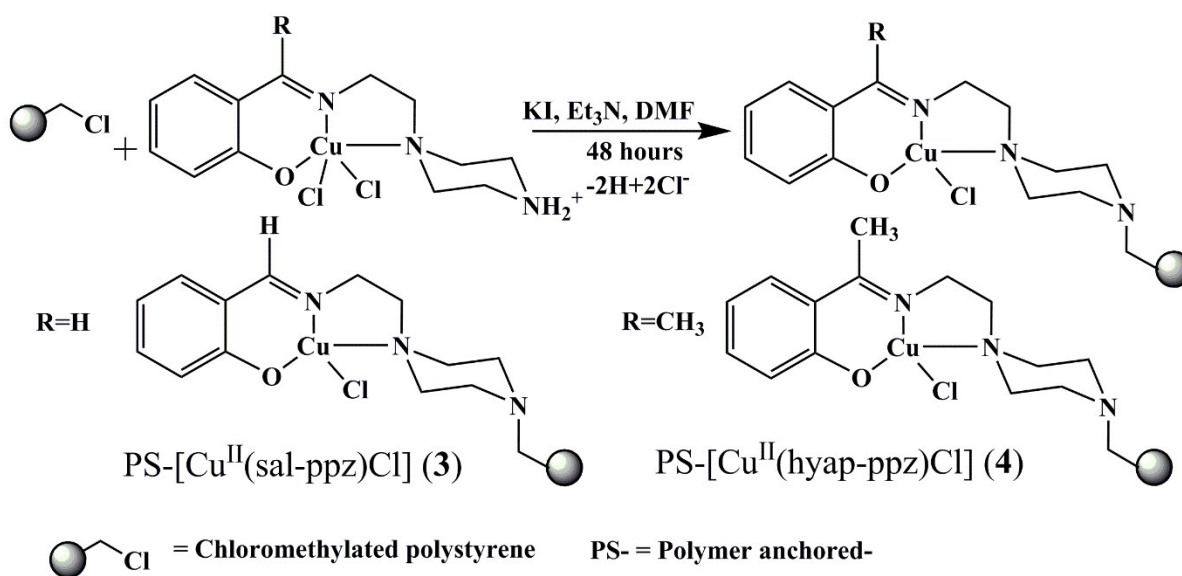
Scheme 3: Synthetic approach for the heterogenization of Cu(II) complexes.

3.0. Results and Discussion

3.1. Molecular structure of complex [Cu^{II}(sal-ppzH) Cl$_2$] (**1**).

Single crystal XRD data analysis shows that the [Cu^{II}(sal-ppzH) Cl$_2$] (**1**)crystallizes in space group P$\bar{1}$, with a distorted square pyramidal geometry around the copper atom. Ellipsoid plot of the **1** is shown in the figure 2. τ-value of the complex is 0.0105 (τ =1 for perfect trigonal bipyramidal

geometry and $\tau= 0$ for perfect squire pyramidal geometry[81]) and tells about the distortion around the metal centre.
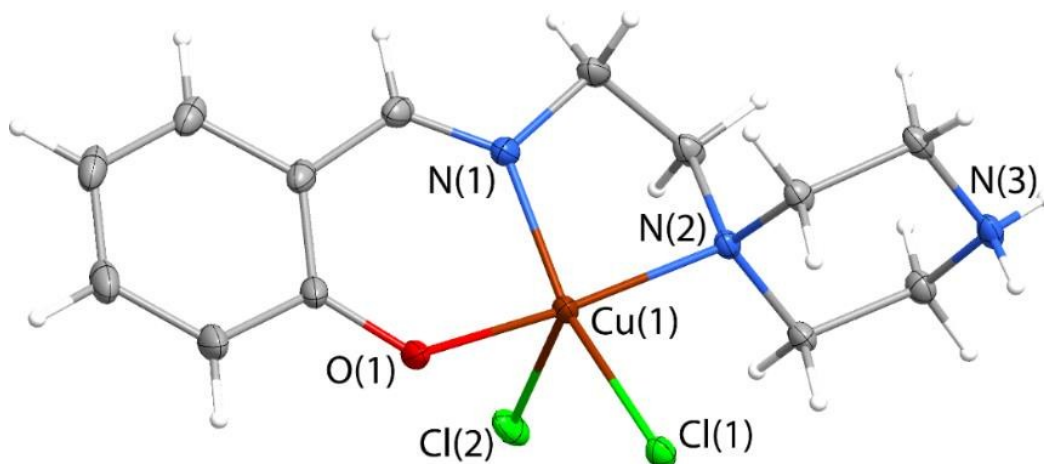

Figure 2: Molecular view of the complex [Cu^{II}(sal-ppzH) Cl_2] (**1**).

Basal plane position are occupied by the phenolate oxygen (O1) from salicylaldehyde ring, one nitrogen (N1) from C=N- group, second nitrogen (N2) from piperazine ring and one chlorine (Cl1) atom. Apical position is occupied by another chlorine (Cl2) atom. Overall negative charge in the first coordination sphere is counterbalanced by the protonation of the piperazine amine group. Cu-Cl(1) bond distance is 2.298 Å whereas apical position chlorine atom (Cl2) and Cu distance significantly longer (2.694 Å).
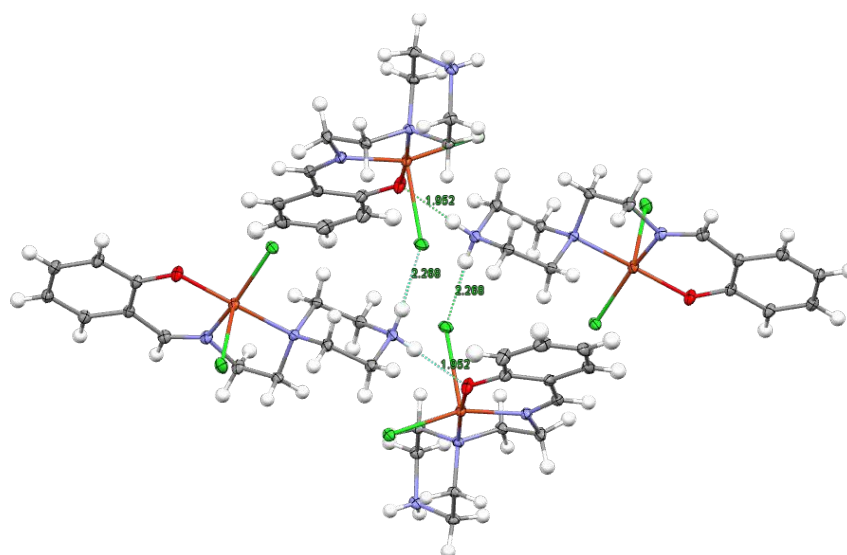

Figure 3: Intermolecular H-bonding in the unit cell of **1**.

Piperazine ring adopted most stable chair conformation whereas protonated piperazine ring amine nitrogen (N3) involved into H-bond formation (figure 3) with the phenolate oxygen (O1) of salicylaldehyde of another molecule (HN-H...O distance is 1.952 Å). Apical position chloride atoms also show a weak H-bonding interaction with the second proton of protonated amine group of piperazine ring (HN-H.....Cl distance 2.268 Å) makes a beautiful molecular association. Selected bond length and bond angles are listed in table S1.

3.2.IR spectral studies

Both the ligands show one broad band in the range of 3369 to 3432 cm^{-1}, due to the presence of $\nu_{(O-H)}$,while the same band present in the corresponding metal complexes in the range of 3413 to 3435 cm^{-1},signify the presence of water of crystallization. All the ligands and metal complexes exhibit medium intensity bands for $\nu_{(N-H)}$in the range of 2926-2945 cm^{-1}. Both the ligands show two sharp bands at 1615-1635 cm^{-1} and 1279-1299 cm^{-1}, because of the $\nu_{(C=N)}$and $\nu_{(C-O)}$respectively. $\nu_{(C=N)}$and $\nu_{(C-O)}$ bands appear in **1** and **2** at lower wave numbers with respect to their counter ligands; indicate the coordination of azomethine (-C=N) nitrogen and phenolic (Ph-O) oxygen to the copper atom. A broad absorption band due to $\nu_{(N-H)wagging}$ is observed in the ligands and in all the metal complexes in the range of 739-759 cm^{-1}. All the polymer anchored metal complexes exhibit the similar spectral pattern like complex **1** and **2** but with reduced intensity because of the polymeric matrix (figure S1). Partial list of important IR spectral data of ligands and metal complexes are shown in the table S2.

3.3.Electronic Spectral data for the ligands and metal complexes

UV-Vis spectra of ligands and Cu(II) complexes were recorded in methanol at room temperature. While UV-Vis spectra of polymer anchored copper(II) complexes were recorded in nujol. Partial list of important spectral data of ligands, copper(II) complexes and polymer anchored copper(II) complexes are listed in table S3.

In methanol, ligand [Hsal-ppz] (**I**) shows three bands at 254, 316 and 405 nm along with a shoulder band at 272 nm. While ligand [Hyap-ppz] **(II),** exhibits two bands at270 and 388 nm and a shoulder band at 324 nm. Absorption bands shown by both ligands in the range of 254 -316 nm are assignable to π-π* transition. Whereas bands appearing in the range of 388-405 nm are indication of the n-π* transition in the ligands. All these bands show a slight hypsochromic shift in the

corresponding copper(II) complexes (figure S2) along with a new sharp band in the range of 222-225 nm.

Complexes $[Cu^{II}(sal\text{-}ppzH)Cl_2]$ (**1**) and $[Cu^{II}(hyap\text{-}ppzH)Cl_2]$ (**2**) show one broad absorption band at 667 nm and 638 nm, respectively (figure 4), assignable to *d-d* transition. Higher extinction coefficient value for **1** (ε_{667} =88, litre mol^{-1} cm^{-1}) in comparison to **2** (ε_{638} =67, litre mol^{-1} cm^{-1}) suggests lower symmetry and maximum distortion in **1** from the ideal square pyramidal geometry than **2**.[82] Polymer anchored metal complexes PS-$[Cu^{II}(sal\text{-}ppz)Cl]$ (**3**) and PS-$[Cu^{II}(hyap\text{-}ppz)Cl]$ (**4**) exhibit similar spectral behavior to that of unanchored metal complexes with reduced absorbance intensity (figure S3). Presence of these absorbance bands, established the existence of copper complexes into the polymeric matrix. However, PS-$[Cu^{II}(sal\text{-}ppz)Cl]$ (**3**) was unable to produce any detectable 238 nm and 667 nm absorbance band, because of very poor loading of the metal complex into the polymer matrix.
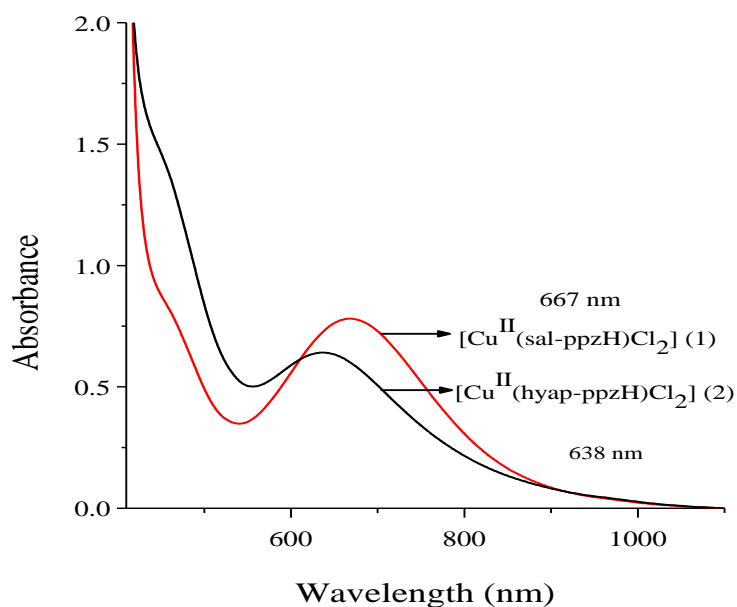

Figure 4: Electronic spectra of 8.837×10^{-3} M methanolic solution of $[Cu^{II}(sal\text{-}ppzH)Cl_2]$ (**1**)(red line) and 9.429×10^{-3} M methanolic solution of $[Cu^{II}(hyap\text{-}ppzH)Cl_2]$ (**2**)(Black line).

3.4. Electrochemical properties

Redox potential of the metal center has an immense role in the catalytic redox reaction. CV measurements were performed by a computerized electrochemical trace analyzer at a scan rate of 0.1 V sec^{-1} in DMF solution containing 0.1 (M) TBAP (tetrabutylammonium perchlorate) as a supporting electrolyte, using a three-electrode configuration (glassy carbon working electrode, Pt counter electrode, and Ag/AgCl as reference electrode). De-aerated solutions were used by purging N_2 gas for 10 min prior to measurements. The whole measurements were automated and controlled through the programming capacity of the apparatus. The solvents used were sufficiently pure and the concentration of the complexes was kept at 0.001 M.
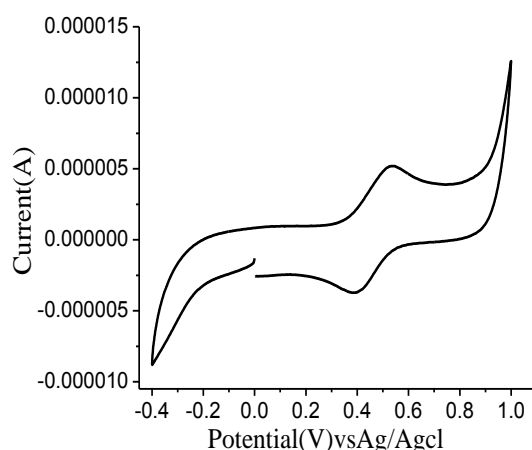

Figure 5: A representative cyclicvoltammogram of **2** with scan rate 0.1 V Sec^{-1} and 0.1 M TBAP in DMF.

Table 2: Electrochemical data for **1** and **2** in DMF solution.

Complex	E^a_p (V)	E^c_p (V)	ΔE_p(V)	$E_{1/2}$ (V)
[Cu^{II}(sal-ppzH)Cl$_2$] (**1**)	0.54	0.40	0.14	0.47
[Cu^{II}(hyap-ppzH)Cl$_2$] (**2**)	0.52	0.37	0.15	0.48

Both complexes show a quasi-reversible cyclic voltamogram corresponding to Cu$^{II/I}$ system (shown in the figure 5) with peak separation ranging from 0.11 V to 0.15 V in DMF solution. Cyclic voltagram of **1** is shown in the figure S4. Approximate formal potential ($E_{1/2}$) of the complexes was calculated by taking an average of peak potentials. Complexes **1** and **2** show $E_{1/2}$ values 0.47V and 0.48V respectively (listed in table 2). Voltagram confirms the successful

formation of Cu^{2+} complexes. Close formal potential indicates similarity of their electronic environments and expecting very close catalytic behaviors.

3.5. Thermogravimetric analysis

Thermal stability of the polymer anchored copper(II) complexes, PS-[Cu^{II}(sal-ppz)Cl] (**3**), and PS-[Cu^{II}(hyap-ppz)Cl] (**4**) were examined by TGA method under nitrogen atmosphere at a temperature rate of 10°C/ min over a temperature range of 33°C to 800 °C. Both of the polymer anchored copper(II) complexes are considerably stable up to 330°C.Complexes **3** and **4** show a negligibly small but progressive weight loss of ~ 3.0 % (up to 328°C)and ~ 6.0 % (up to 320°C) respectively due to the physically adsorbed gases and water molecules. **3** exhibits maximum weight loss (76.71 %) in the temperature range 328°C-466°C while complex **4** displays the maximum weight loss (68.25 %) in the range of 320°C-470°C, which is attributed to the decomposition of polymeric matrix and metal complex backbone (figure 6).
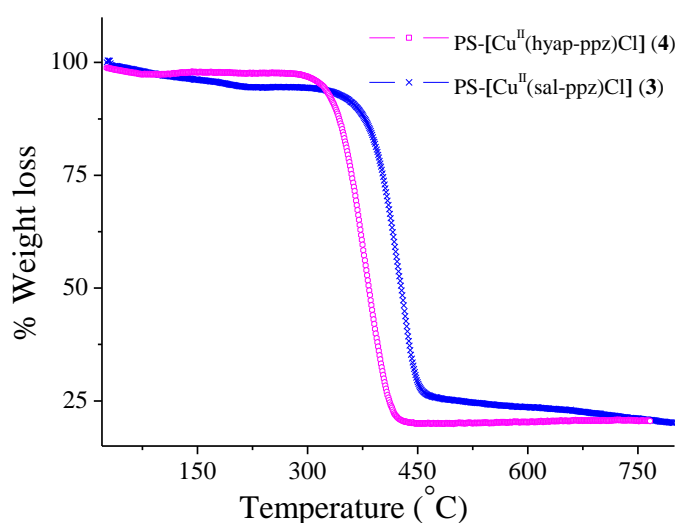

Figure 6: Thermogravimetric temperature vs. % weight loss plot for PS-[Cu^{II}(sal-ppz)Cl] (**3**), and PS-[Cu^{II}(hyap-ppz)Cl] (**4**).

3.6.SEM-EDX Analysis

Surface morphological changes among the pure chloromethylated polystyrene, polymer anchored copper(II) complexes **3** and **4** were examined by scanning electron microscopic analysis (SEM)(shown in the Figure 7). Copper(II) complexes anchored polymer bead shows no significant morphological changes. Slightly roughening in the outer surface of the polymer bead may be due

to incorporation of metal complexes into the polymeric matrix as well as the frictional force experienced during the process of heterogenization. Metal complexes anchored polymer bead looks little shinny because of the presence of solvent molecules during the analysis.
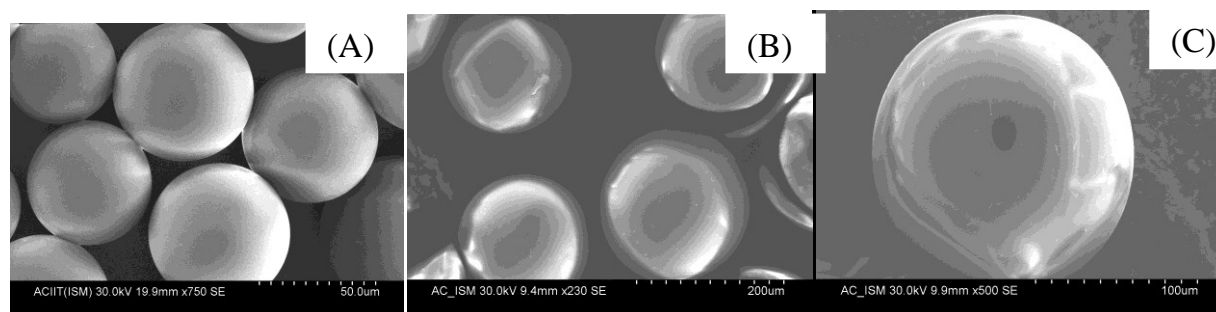

Figure 7: SEM image of (A) Pure Chloromethylated polystyrene (B) PS-[Cu^{II}(sal-ppz)Cl] (**3**) and (C) PS-[Cu^{II}(hyap-ppz)Cl] (**4**)

Energy Dispersive X-ray (EDX) analysis of the copper(II) complexes anchored polymer bead (shown in the figure 8) indicates the presence of Cu along with C, N and O, hence confirms the successful anchoring of copper complexes into the polymeric matrix of chloromethylated polystyrene. EDX analysis of complex **3** and **4** also shows the presence of Cl signal, signifying the very dilute dispersion of copper(II) complexes into the polymeric matrix. Metal loading calculated from EDX analysis for complex **3** and **4** is 1.87 % and 2.75 % respectively. The actual concentration of copper in the polymer matrix was estimated by AAS analysis which shows the values 0.07836% (0.01233 mmolg^{-1}) and 0.399% (0.0628 mmolg^{-1}) for complex **3** and **4** respectively.
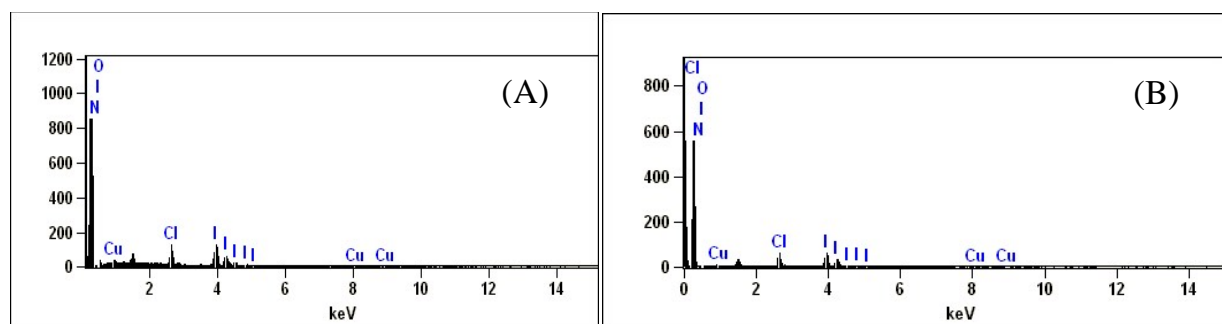

Figure 8: Energy dispersive X-ray analysis graphs of (A) PS-[Cu^{II}(sal-ppz)Cl] (**3**) and (B) PS-[Cu^{II}(hyap-ppz)Cl] (**4**)
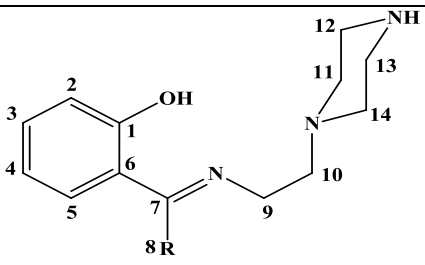
3.7. ^{1}H and ^{13}C NMR Spectral studies

Molecular structure of Schiff-base ligands [Hsal-ppz] (**I**) and [Hyap-ppz] (**II**) was confirmed by ^{1}H-NMR analysis. ^{1}H-NMR spectra (figure S5 and S6) of the ligands were recorded in CDCl$_3$ and spectral data are summarized in the table 3. Ligand [Hsal-ppz] (**I**) shows two broad signals, one appearing at 4.98 ppm assigned to -NH proton while another broad signal appearing at 13.27 ppm may be due to the -OH proton which is deshielded by intramolecular H-bonding with the imine-N. Similarly, in ligand [Hyap-ppz] (**II**), -NH and -OH proton signals are appearing at 5.87 ppm and 16.20 ppm respectively. Ligand **I** shows one sharp singlet at 8.26 ppm because of -CH=N proton, along with four aromatic proton (6.78-7.23 ppm) and twelve aliphatic protons (2.46-3.67 ppm) within the expected region.[Hyap-ppz] (**II**) shows four aromatic proton in the range of 6.66-7.43 ppm and twelve aliphatic proton in the range of 2.45-3.62 ppm along with one sharp singlet signal at 2.26 ppm due to the presence of -CH$_3$protons.

Table 3:^{1}H-NMR spectral data of ligands (δ in ppm)

Compounds	- NH	-OH	-CH=N	Aromatic	Aliphatic	-CH$_3$
[Hsal-ppz] (**I**)	4.98 (s, 1H)	13.27 (s, 1H)	8.26 (s, 1H)	6.78 (t, 1H), 6.88 (d, 1H), 7.15 (d, 1H), 7.22 (t, 1H)	2.46 (s, b, 4 H), 2.55 (t, 2H), 2.63 (m, 2H), 2.93(t, 2H), 3.65 (q, 2H)	-
[Hyap-ppz] (**II**)	5.87 (s, 1H)	16.20 (s, 1H)	-	6.68(t, 1H), 6.85 (d, 1H), 7.19 (t, 1H), 7.43 (d, 1H)	2.45 (s, b, 4H), 2.68(t, 2H), 2.84 (s, b, 4H), 3.61 (t, 2H)	2.26 (s, 3H)

Ligands' backbone was further confirmed by ^{13}C NMR spectral studies. The relevant spectral data are collected in table 4. CDCl$_3$ was used to record the ^{13}C NMR spectra of the ligands. All spectra are in good agreement with the proposed ligands structure. Ligand **I** ([Hsal-ppz]) shows two signals, one at 166.51 ppm due to phenolic carbon (C1) (Ph-OH) and another at 164.01 ppm because of azomethine carbon (C7). Likewise C1 and C7 signals appear in [Hyap-ppz] (II) at 174.40 and 169.48 ppm respectively. In ligand **I,** aromatic carbon atoms show four signals in the range of 133.02-117.68 ppm (C2- C6) while all the six aliphatic carbon atoms exhibit four signals in the range of 57.93-44.02 ppm (C9-C14). Ligand **II** shows five aromatic signals (134.05-115.20 ppm) and four aliphatic signals (57.39-44.08 ppm) within the expected region, along with a signal for -CH$_3$at 37.11 ppm (table 4).

Table 4: The position of the carbon signals in the [13] C-NMR spectra of the ligands(δ in ppm).

Ligands	
	  ^{13}C-NMR signals (ppm)
R=H [HSal-ppz] **(I)**	166.51 (C1), 164.01 (C7),133.02 (C4), 131.91 (C3 & C5), 11.18 (C6), 117.68 (C2), 57.93 (C9), 54.16 (C10), 51.11 (C12 & C13), 44.02 (C11 & C14).
R=CH$_3$ [Hyap-ppz] **(II)**	174.40 (C1), 169.48 (C7), 134.05 (C4), 128.99 (C5), 120.58 (C3), 117.16 (C6), 115.20 (C2), 57.39 (C9 & C10), 53.28 (C12 & C13), 44.08 (C14 & C11), 37.11 (C8)

3.8. EPR Spectral Studies

Room temperature X-band EPR spectra of **1** and **2** in DMSO were represented in the figure 9. They are characteristic of a typical axially symmetric paramagnetic centre. For **1,** g‖= 2.249 and g⊥ = 2.051. While for **2,** g‖ = 2.262 and g⊥ = 2.052. In solution both complexes show axial symmetric g tensor parameters g‖> g⊥>g(2.0023) indicating that the unpaired electron lies in a dx^2-y^{2}ground state orbital. Absence of well resolved hyperfine lines in their spectra indicate a situation usually observed in the case where copper-copper interaction is present.[83,84]

Lack of half-field transition (around 1600 G) indicates that both of the complexes exist as monomer in the solution. In axial symmetry, G values which are related to g by G = (g‖-22)/(g⊥-2) = 4. Complexes [Cu^{II}(sal-ppzH)Cl$_2$] (**1**) and (B) [Cu^{II}(hyap-ppzH)Cl$_2$] (**2**) show G values 4.88 and 5.04 respectively which indicates negligible copper-copper magnetic interaction.[85]
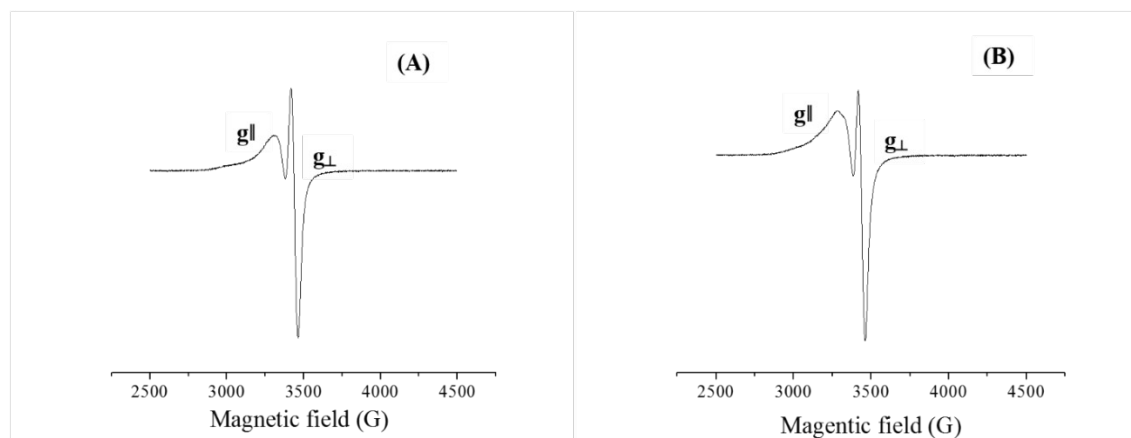
Figure 9: X-band EPR spectra of (A) [Cu^{II}(sal-ppzH)Cl$_2$] (**1**); (B) [Cu^{II}(hyap-ppzH)Cl$_2$] (**2**) in DMSO at room temperature.

X-band EPR spectra of the polymer anchored metal complexes PS-[Cu^{II}(sal-ppz)Cl] (**3**) and PS-[Cu^{II}(hyap-ppz)Cl] (**4**) at 77K are reproduced in figure 10. The calculated principle components of g tensor for **1** are $g_{av}\| = 2.319$ and $g\perp = 2.038$ while **2** shows $g_{av}\| = 2.312$ and $g\perp = 2.043$. Figure 10 is characteristics of monomeric Cu^{2+} centre and typical axial symmetry EPR spectra may be due to square pyramidal geometry of the molecule shown in figure 2. The hyperfine structure, due to the interaction of electron spin S=1/2 with Cu^{2+} nuclear spin values S=3/2, is well resolved in the spectra. Well resolved hyperfine structure implies the fact that copper complexes are well dispersed into the polymer matrix where the probability of copper-copper magnetic interaction is negligible. Additionally EPR spectrum of **1** at 77K exhibits a poorly resolved super hyperfine splitting in the perpendicular region probably due to the interaction of Cu^{2+} with nitrogen atom.
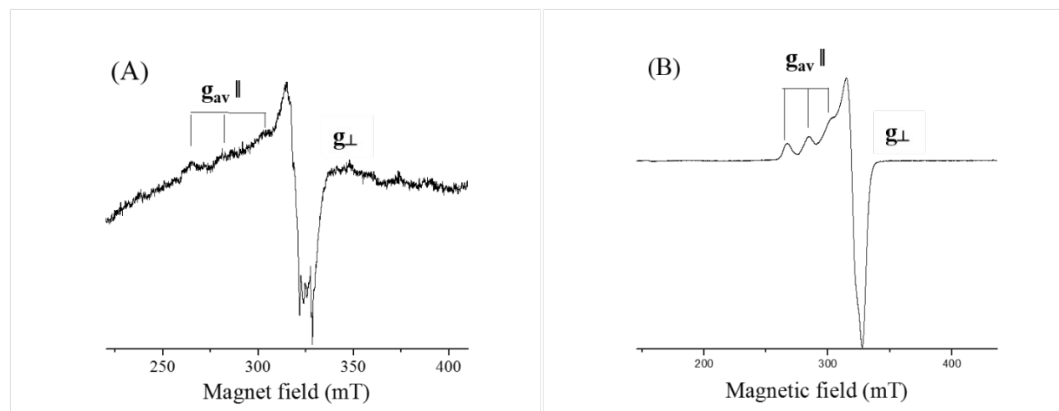

Figure 10: X-band EPR spectra of polymer-anchored complexes PS-[Cu^{II}(sal-ppz)Cl] (**3**) and PS-[Cu^{II}(hyap-ppz)Cl] (**4**) at 77K.

3.9. Computational Studies

DFT calculations were performed to understand the structural and chemical behavior of the synthesized complexes. In spite of our repeated efforts, we could not isolate suitable crystals for X-ray diffraction studies of the complex **2**. Hence X-ray refinement data of the mononuclear [Cu^{II}(sal-ppzH)Cl$_2$] (**1**) complex was taken as an initial guess for the liquid phase geometry optimization of the two complexes. Selected bond lengths and bond angles of the calculated and experimental geometry are mentioned in the table 5. Very close agreements between the experimental and calculated geometry were observed. Most of the calculated bond lengths are little elongated than the X-ray crystallographic data, because X-ray crystal diffraction was applied in the solid state while theoretical calculations were performed in the liquid phase. For the very same reason there is slight deviation in bond angles also. Frequency calculations were performed using similar method and basis set to check the accuracy of the optimization process. Absence of imaginary frequency ensures minimum global energy of the optimized geometry. Geometry optimized structure of the complexes were shown in the figure 11. All the complexes adopt a distorted square-pyramidal geometry as suggested by the X-ray refinement data of the mononuclear [Cu^{II}(sal-ppzH)Cl$_2$] (**1**).

Table 5: Geometry optimized parameters for the **1** and **2** computed at DFT/ UB3LYP/LanL2dz𝑈 6-311G (d,p) level of theory.

Sl. No.		Bond distance (Å)		
		Experimental data of **1**	Calculated data of**1**	Calculated data of**2**
1	Cu(1)-O(1)/N4	1.927	1.949	1.92787
2	Cu(1)-Cl(1)	2.298	2.405	2.42564
3	Cu(1)-Cl(2)	2.694	2.759	2.74310
4	Cu(1)-N(1)	1.945	2.005	2.03184
5	Cu(1)-N(2)	2.089	2.194	2.17366

Sl. No.		Bond angle (°)		
		Experimental data of **1**	Calculated data of **1**	Calculated data of **2**
1	Cl(1)-Cu(1)-N(1)	158.14	159.702	160.715
2	Cl(2)-Cu(1)-N(1)	98.74	97.549	97.073
3	O(1)/N4-Cu(1)-N(2)	174.24	169.764	166.707
4	Cl(1)-Cu(1)-Cl(2)	102.98	102.196	101.908
5	Cl(1)-Cu(1)-N(2)	92.60	91.996	91.235
6	N(1)-Cu(1)-N(2)	83.71	82.720	84.293
7	O(1)/N4-Cu(1)-N(1)	92.71	91.009	90.054
8	O(1)/N4-Cu(1)-Cl(1)	89.05	91.136	90.168
9	N(1)-Cu(1)-Cl(2)	98.74	97.549	97.073
10	O(1)/N4-Cu(1)-Cl(2)	91.92	97.226	99.457
11	N(2)-Cu(1)-Cl(2)	93.08	91.632	93.185
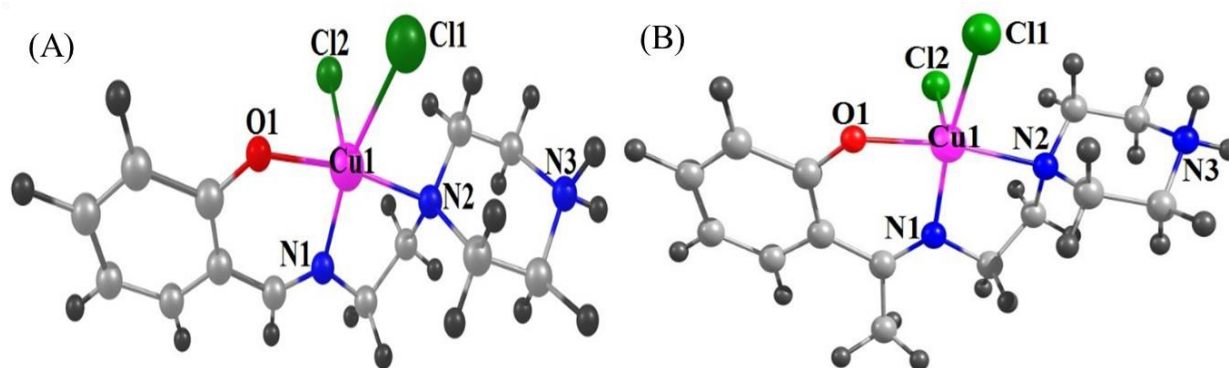
Figure 11: Optimization structure of (A) [Cu^{II}(sal-ppzH)Cl$_2$] (**1**) and (B) [Cu^{II}(hyap-ppzH)Cl$_2$] (**2**)calculated at DFT/ UB3LYP/LanL2dz$U$6-311G (d, p) level of theory.

We have also calculated some of the quantum chemical properties of the complexes **1** and **2**, by using mixed basis set LANL2DZU6-311G (d,p) and listed in the table 6. HOMO and LUMO are the two most important frontier molecular orbital in a molecule (figure 12 and 13). HOMO is the highest molecular orbital which carry electrons. So, the Ionization Potential (IP), which is an indication of electron donating ability, is directly related to the HOMO energy. Similarly, LUMO

is the highest empty molecular orbital which can capable of accepting electrons. Thus LUMO energy is related to the electron affinity (EA) of the molecules. Chemical stability[86] of a molecule is therefore decided by the HOMO-LUMO energy gap.
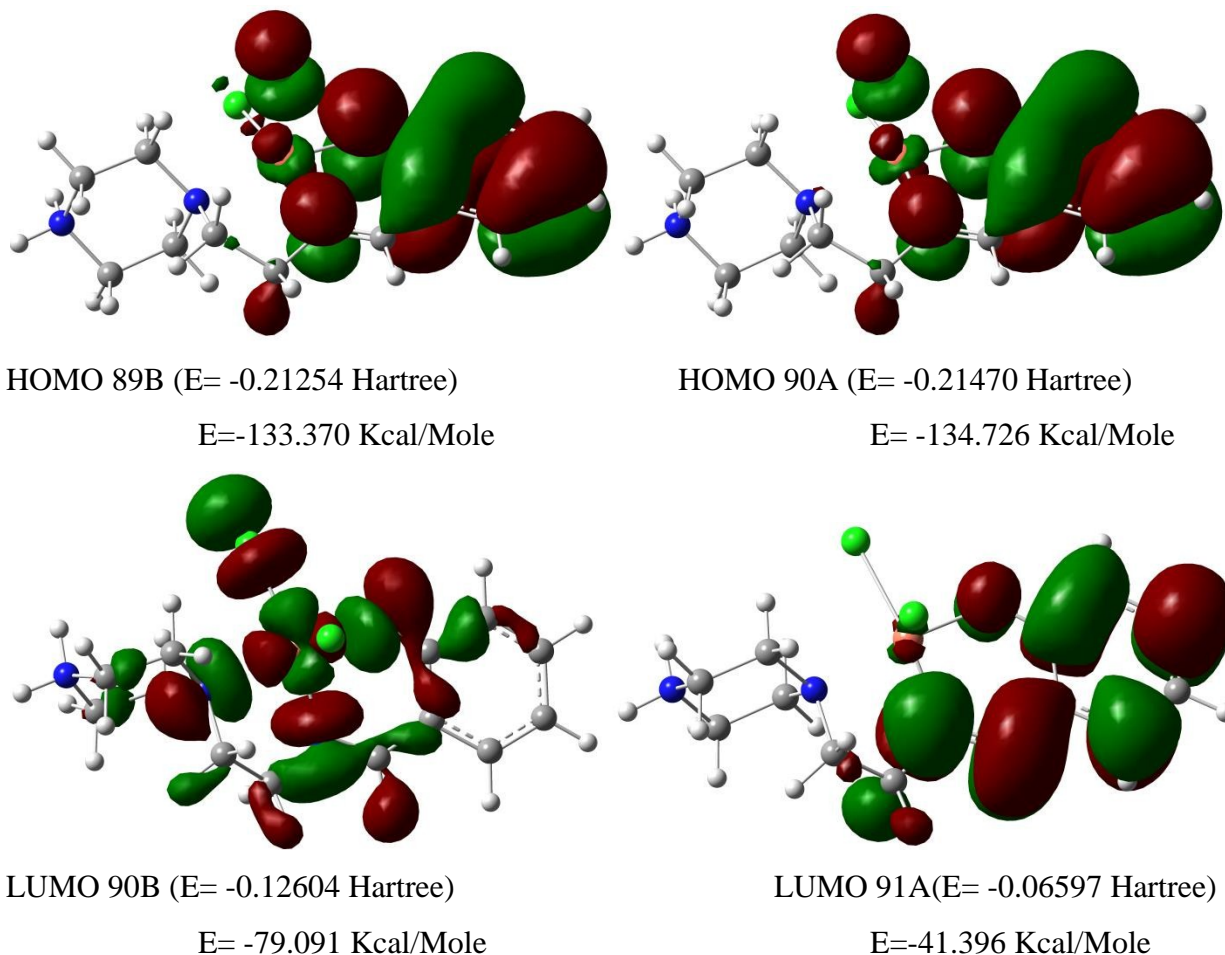

HOMO 89B (E= -0.21254 Hartree)

E=-133.370 Kcal/Mole

HOMO 90A (E= -0.21470 Hartree)

E= -134.726 Kcal/Mole

LUMO 90B (E= -0.12604 Hartree)

E= -79.091 Kcal/Mole

LUMO 91A(E= -0.06597 Hartree)

E=-41.396 Kcal/Mole

Figure 12: Frontier Molecular orbitals of [Cu (sal-ppzH) Cl$_2$] (**1**)

HOMO 93B (E= -0.21079 Hatree)

E=-132.272 Kcal/Mole

HOMO 94A (E= -0.21225 Hatree)

E=-133.188 Kcal/Mole

LUMO 94B (E= -0.12171 Hatree)   LUMO 95A(E= -0.06162 Hatree)

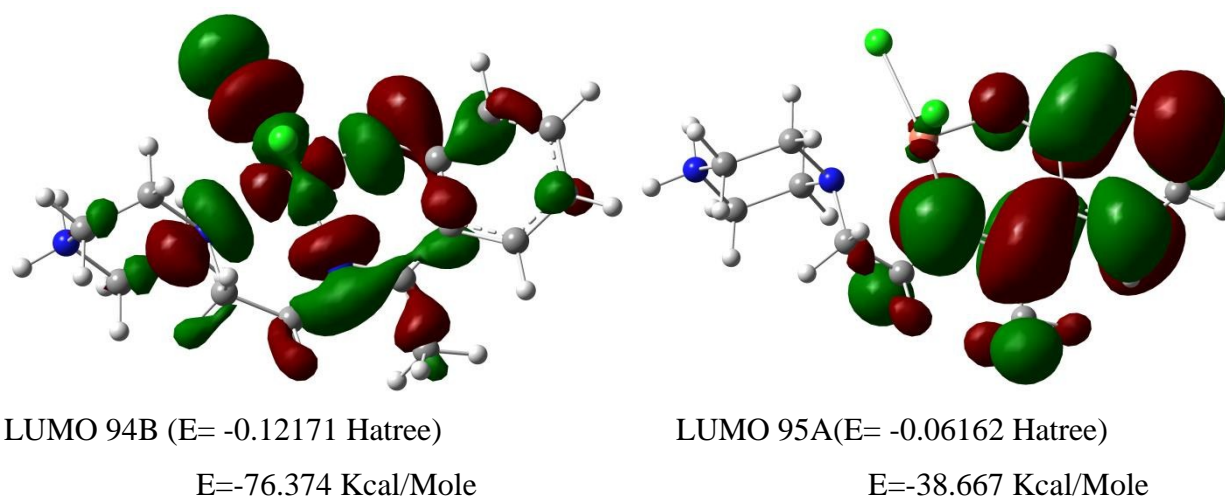E=-76.374 Kcal/Mole   E=-38.667 Kcal/Mole
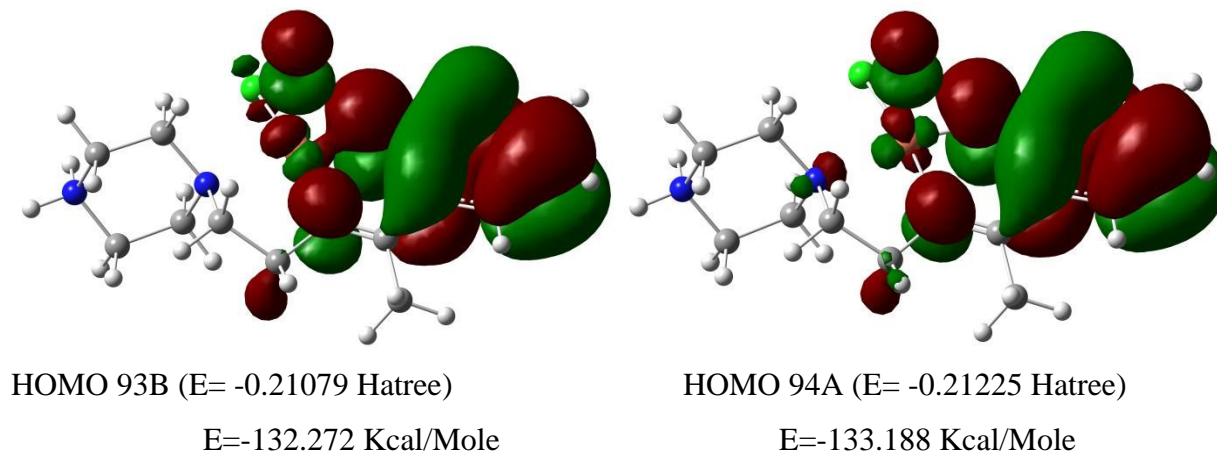
Figure 13: Frontier Molecular orbitals of [Cu^{II}(hyap-ppzH) Cl$_2$] (**2**)

HOMO-LUMO energy gap is quite important in determining a number of molecular properties, like electrical transport properties, electronegativity, chemical hardness, chemical softness, electrophilicity index etc.[87]

Table6:Selected quantum chemical properties calculated by using DFT /UB3LYP methods with mixed basis set LANL2DZ*U*6-311G (d,p).

| SL No	Parameters	**1**	**2**
1	HOMO (Kcal/mole) (IP)	-134.73	-133.19
2	LUMO (Kcal/mole) (EA)	-79.09	-76.37
3	|ΔE| (energy gap) (Kcal/mole)	55.64	56.81
4	χ(Kcal/mole) (Electronegativity)	106.91	104.78
5	η (Kcal/mole)(Chemical hardness)	27.82	28.41
6	ξ(Kcal/mole) (softness)	0.017974	0.017601
7	ψ(Kcal/mole) (electrophilicity index)	205.44	193.25

From table 6 it is clear that the ionization potential of **2** (-76.37 Kcal/Mole) is less in comparison to **1** (-79.09 Kcal/Mole). Compound **2** also shows large HOMO-LUMO energy gap (56.81 Kcal/Mole) and highest chemical hardness values (28.41 Kcal/mole) which indicates its larger

chemical stability and high chemical hardness in comparison to **1**. In summary, **2** is marginally more stable but easily convertible to the Cu(III) than **1.**

3.10. Catalytic studies

3.10.1. Catalytic oxidation of 3,5-DTBC

Because of its low redox potential, 3,5-DTBC is easily oxidized to 3,5-DTBQ (Scheme 4)[88] which is stable and shows strong absorbance band at $\lambda_{max} = 400$ nm in methanol.
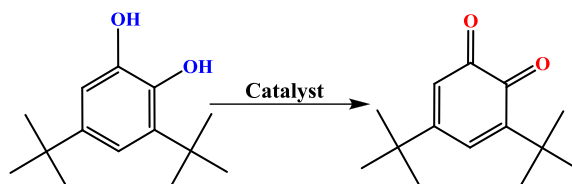
Scheme 4: Catalytic conversion of 3,5-DTBCto 3,5-DTBQ.

Catalytic conversion of 3,5-DTBC to 3,5-DTBQ by $[Cu^{II}(sal\text{-}ppzH)Cl_2]$ (**1**) and $[Cu^{II}(hyap\text{-}ppzH)Cl_2]$ (**2**) in presence of dilute hydrogen peroxide were evaluated by UV-Vis spectrophotometer in methanol by observing the increase of the 400 nm absorption band as a function of time under pseudo first order condition (figure 1).

Formation of 3,5-DTBQ was also detected by thin layer chromatography technique using authentic sample of 3,5-DTBQ. In absence of catalyst no conversion of 3,5-DTBQ was observed. A fixed concentration of H_2O_2 is essential in the catalytic cycle. To optimized the amount of H_2O_2, four different amount 0.25 ml, 0.50 ml, 1.0 ml and 1.25 ml of 1.0×10^{-1} M H_2O_2 were used for a fixed amount of 3,5-DTBC (1.0 ml, 2.85×10^{-2} M) and catalyst **2** (0.5 ml, 1.0×10^{-4} M solution) in a quartz cuvette (total volume of reaction mixture was 3.0 ml in every batch of reaction) at room temperature and pressure (Plot S1) for 30 min. With increasing the amount of H_2O_2 from 0.25 ml to 0.50 ml, product absorbance value slightly increases from 0.705 to 0.849. While a large jump in product absorbance value (1.43) was observed with using 1.0 ml of H_2O_2. Further increasing the amount from 1.0 ml to 1.25 ml product absorbance (1.63) values increases marginally. Hence 1.0 ml of 1.00×10^{-1} M H_2O_2 in 3 ml of solution (i.e. 3.33×10^{-2} M H_2O_2) was considered as optimum for catalytic oxidation 3,5-DTBC. To evaluate the efficiency of the catalyst we have determined the kinetics of the oxidation of 3,5-DTBC by initial rate method by monitoring the growth of the 400 nm band as a function of time.

In this process we have reacted 0.5 ml 1×10^{-4} M solution of catalysts with 1.0 ml of six different substrate concentrations of 1×10^{-1} M, 1×10^{-2} M, 2×10^{-2} M, 4×10^{-2} M, 6×10^{-2} M and 8×10^{-2} M in the presence of 1 ml 1×10^{-1} M H_2O_2 and 1.0 ml of methanol for a maximum time period of 10 minutes . At the low substrate concentration, **1** and **2** shows the first order rate dependence while at high substrate concentration, zero order or saturated kinetics was found for both complexes (Shown in plot 2). Rate dependence on the substrate concentration signifies a substrate–catalyst adduct formation in the initial steps of the reaction. The rates of the reactions versus substrate concentration data were fitted on the basis of Michaelis-Menten approach of enzyme kinetics and linearized by means of Lineweaver-Burk plot to calculate the various kinetic parameters (listed in table 7) like V_{max}, K_m, K_{cat} etc. for these catalysts.
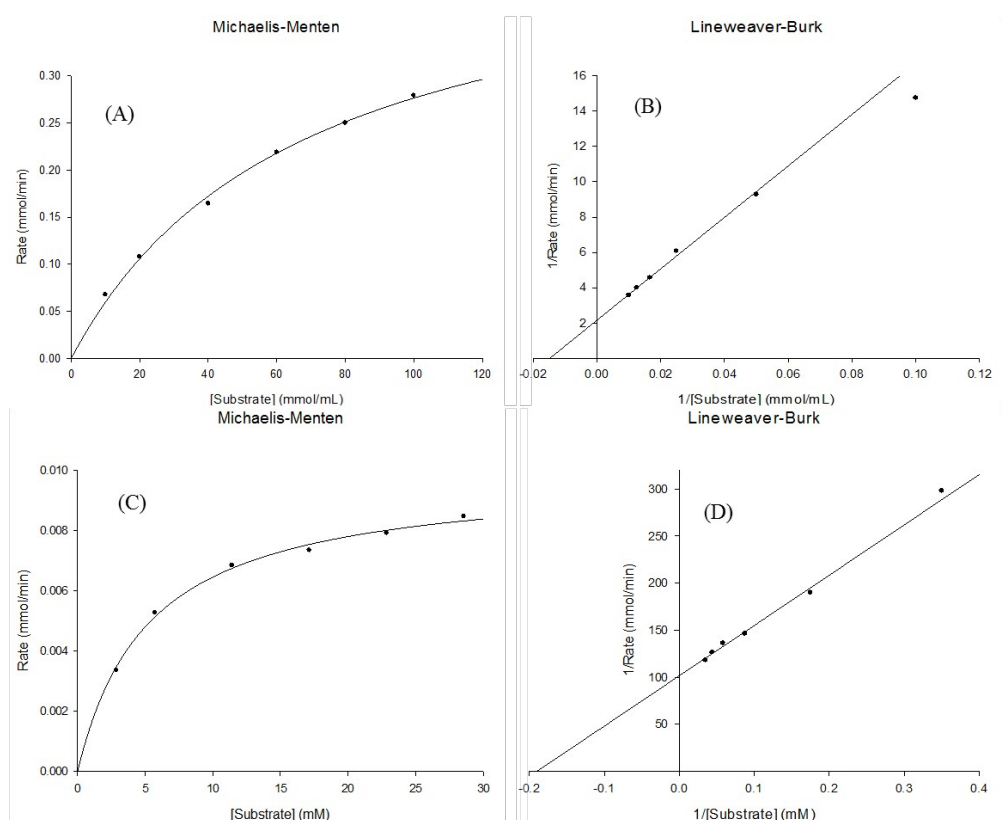
Plot 2: Initial rate versus substrate concentration for the oxidation of 3,5-DTBC. (A) Kinetic curves catalyzed by [Cu(sal-ppzH)Cl$_2$] (**1**) monitored at 400 nm in methanol (B) Lineweaver-Burk plot of the same reaction catalyzed by **1** (C) Kinetic curves catalyzed by [Cu(hyap-ppzH)Cl$_2$](**2**) and (D) Lineweaver-Burk plot of the same reaction catalyzed by **2.** Symbol and solid lines represent the observed and simulated kinetic profile respectively. (Reaction conditions: 1 ml substrate (1×10^{-1} M,

1×10^{-2} M, 2×10^{-2} M, 4×10^{-2} M, 6×10^{-2} M, 8×10^{-2} M) was reacted with 1 ml H_2O_2 (1×10^{-1} M) and 0.5 ml catalyst (1×10^{-4} M) in presence of 1 ml MeOH.)

Table 7: Kinetic data for the oxidation of 3,5-Di-*tert*-butylcatechol catalyzed by various copper complexes.

	V_{max} (mmolmin^{-1})	K_{cat} (mmolmin^{-1})	K_m (mmol)	K_{cat}/K_m (min^{-1})
[Cu(sal-ppzH)Cl$_2$] (**1**)	9.85×10^{-3}	1.970×10^2 (1.182×10^4mmol)/h	5.3	3.718×10^1
[Cu(hyap-ppzH)Cl$_2$](**2**)	2.389×10^{-2}	4.801×10^2 (2.880×10^4 mmol)/h	4.2	1.143×10^2

From table 7, it is evident that the **1**and **2** shows maximum rate (V_{max}) at saturating substrate concentration for 3,5-DTBC oxidation is9.85×10^{-3} mmolmin^{-1} and 2.389×10^{-2} mmolmin^{-1} respectively. Quite larger K_m values for **1** and **2** indicates their less efficient binding with the substrate hence require higher substrate concentration to reach the V_{max}. Complex **1** shows an enhanced turn over frequency of 1.182×10^4 mmolh^{-1} while complex **2** exhibit K_{cat} 2.880×10^4 mmolh^{-1},which are highest amongst the so far reported by monomeric copper(II) complexes and two to three times more than the previously reported by Krebs et al., Neves et al., Monzani et al., and Vittal et al.[89-98].

3.10.1.1. *Reactivity in solution and possible reaction pathway.*

Catechol oxidase uses molecular oxygen as an active oxidant for the catalytic conversion of o-phenols to the corresponding o-quinones. In the current reaction condition, molecular oxygen has little effect (dissolved oxygen under 1 atm pressure and room temperature) but presence of hydrogen peroxide does the job efficiently. For mononuclear and binuclear complexes A. Mukherjee et al.[22] have suggested a number of mechanistic pathways for catechol oxidase enzyme. Several model complexes follow the path which produces two molecules of *o*-quinone and water is followed by the enzyme catechol oxidase.[99,100] Many model complexes follow a different pathway where a peroxo intermediate is responsible for the production of *o*-quinone along with the hydrogen peroxide.[101-110] Based on DFT calculations, M.K. Panda et al[111] suggested that the rate determining steps for the oxidation of catechol to o-quinone is the intramolecular proton

transfer in the superoxo species yielding a peroxo intermediate which is also supported by Á. Kupán et al.[112] In present studies instead of aerial oxygen we have used hydrogen peroxide as an oxidant which might change the course of the catalytic reaction sequence little different from the reported one.

For the identification of possible intermediate species we have reacted complex **1** with H_2O_2 in methanol and monitored by UV-Vis spectrophotometer. Spectral changes were observed after the successive addition of 1-drop portion of 3.67×10^{-2} M H_2O_2 into a 20 ml 2.5×10^{-4} M methanolic solution of $[Cu^{II}(\text{sal-ppzH})Cl_2]$ (**1**). Gradual addition of 1-drop portion of 3.67×10^{-2} M H_2O_2 makes the disappearance of the 300 nm shoulder band while 240 nm, 265 nm and 368 nm band gains its intensity; among them 265 nm shows a slight hypsochromic shift (figure 14) and 368 nm band shows slight bathochromic shift. Complex **2**, also undergoes similar spectral changes while interact with H_2O_2.
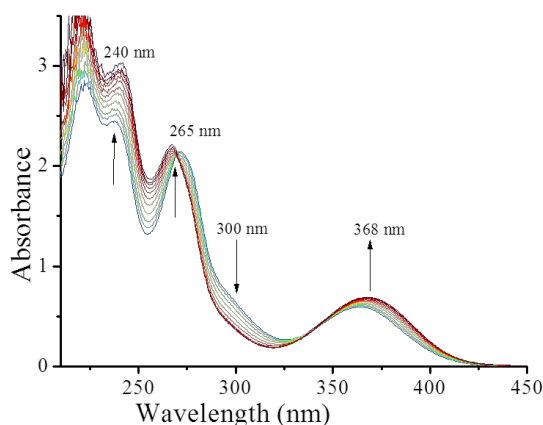

Figure 14: The spectral changes observed after the successive addition 1-drop portion of 3.67×10^{-2} M H_2O_2 into 20 ml of 2.5×10^{-4} M methanolic solution of $[Cu^{II}(\text{sal-ppzH})Cl_2]$ (**1**). The spectra were recorded every 5 min.

Progressive addition of 1-drop portion of 3.67×10^{-2} M H_2O_2 into 20 ml of 9 .429$\times 10^{-3}$ M solution of $[Cu^{II}(\text{hyap-ppzH})Cl_2]$ (**2**) causes the disappearance of the 638 nm band (figure 15). All the changes suggested the formation of Cu(III)-peroxo species in the solution.
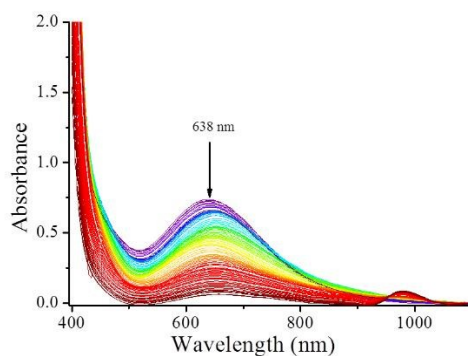
Figure 15: Electronic absorption spectra of complex [Cu^{II}(hyap-ppzH)Cl_2] (**2**) were recorded in methanol. The spectral changes recorded during the successive addition of 1 drop portion of 3.67×10^{-2} M H_2O_2 into a 20 ml of 9.429×10^{-3} M methanolic solution of **2.**

So far at least three different types of peroxo-intermediates, namely side-on Cu^{III}–(μ-η^2-peroxido)–Cu^{III}, bis(μ-oxido–Cu^{III}), and Cu^{III}–O–O–H have been reported during the catalytic reaction.[113, 114] Because of the presence of labile –Cl groups in the monomeric structure of the complex **1** and **2**, formation of Cu^{III}–(η^2-side on peroxo) is expected.

UV-Vis spectrophotometer was also used to monitor the interaction of 3,5-Di-*tert*-butylcatechol with active peroxo species Cu^{III}–(η^2-side on peroxo). Initially, Progressive addition of 1 drop portion of 1.0×10^{-1} M H_2O_2 into the freshly prepared 20 ml 1.0×10^{-4} M methanolic solution of **2,** makes appearance of a new band at around 358 nm, (shown in the inset of figure 16) probably due to the formation of peroxo species (**A**). During this transformation, pH change is also observed by drop-wise mixing of 5 ml 3.96×10^{-1} M H_2O_2 into 10 ml 1.833×10^{-4} M acetonitrile solution of **2** (display pH 5.42) which brings down the pH slowly at 3.40 because of the fact that H_2O_2 addition causes release of H^+ into the solution along with the generation of peroxo species (**A**). ESI-MS spectrum (figure S10) of a methanolic solution of **1** mixed with H_2O_2, exhibits a m/z signal of (M+H) = 329.07, while a signal of m/z = 342.87 (figure S11) observed in the H_2O_2 mixed methanolic solution of **2**. The *m/z =* 329.07 corresponds mass (M+H) of η^2-side on peroxo copper complex of **1** [Cu^{III}(O_2)(sal-ppzH)] and *m/z =* 342.87 represents the mass (M+) of η^2-side on peroxo copper complex of **2** [Cu^{III}(O_2)(hyap-ppzH)]. It clearly indicates the generation of η^2-side on peroxo species (**A**) by the interaction of H_2O_2 with catalyst during the course of reaction.

In the second step, gradual addition of 1 drop portion of methanolic solution of 6.0×10^{-2} M 3,5-DTBC into the above solution causes the appearance of two new bands, one at 290 nm and other at 400 nm along with the disappearance of the 358 nm band. Disappearance of 358 nm band implies the reduction of η^2-side on peroxo Cu^{3+} into the native form (Cu^{2+}) by converting one molecule of 3,5-DTBC into one molecules of 3,5-DTBQ. Formation of the 3,5-DTBQ appears as a new band at 400 nm. Variation in pH during oxidation of 3,5-DTBC by the active peroxo species (**A**) was monitored. Addition of 5 ml 5.698×10^{-2} M methanolic solution of 3,5-DTBC into the solution containing η^2-side on peroxo Cu^{3+} [$Cu^{III}(O_2)$(hyap-ppzH)] (pH=3.4) causes rise of the solution pH and reaches at a maximum of pH = 3.98. Probably, conversion of 3,5-DTBC to 3,5-DTBQ causes depletion of H^+ from solution during oxidation by catalyst as shown in the scheme 5. By reacting with H_2O_2, native catalyst transform into the active catalyst (**A**) which releases the H^+ into the solution and causes fall down of the pH value and finally attaining a constant pH of 3.56. Repeating the addition of another 5 ml 5.698×10^{-2} M 3,5-DTBC in the above reaction mixture causes similar effect as discussed earlier, indicating the existence of catalytic cycle. The variation of pH during the catalytic cycle was recorded and mentioned in figure S9. To confirm the oxidation state of the active copper peroxo species in solution, changes in the EPR spectra were recorded during the gradual addition of dilute 30% hydrogen peroxide solution into the DMSO solution of [Cu^{II}(sal-ppzH)] (**1**) (shown in the figure S14). It is evident from the figure S14 that EPR spectral intensity decreases with stepwise addition of dilute 30 % hydrogen peroxide into DSMO solution of **1,** indicating the formation of EPR silent Cu^{3+} peroxo species. All of the above experimental findings suggest that η^2-side on peroxo Cu^{3+} complex [$Cu^{III}(O_2)$(L)] is the main species responsible for the oxidation of 3,5-DTBC to the corresponding quinone. The intramolecular proton transfer is believed to be the overall rate-determining step of the catalytic reaction[111]. Based on UV-Vis spectral studies, ESI-MS analysis, EPR and pH-metric titration a schematic diagram for the oxidation of 3,5-DTBC by the catalysts at room temperature and pressure in presence of H_2O_2 is presented in the Scheme 5.
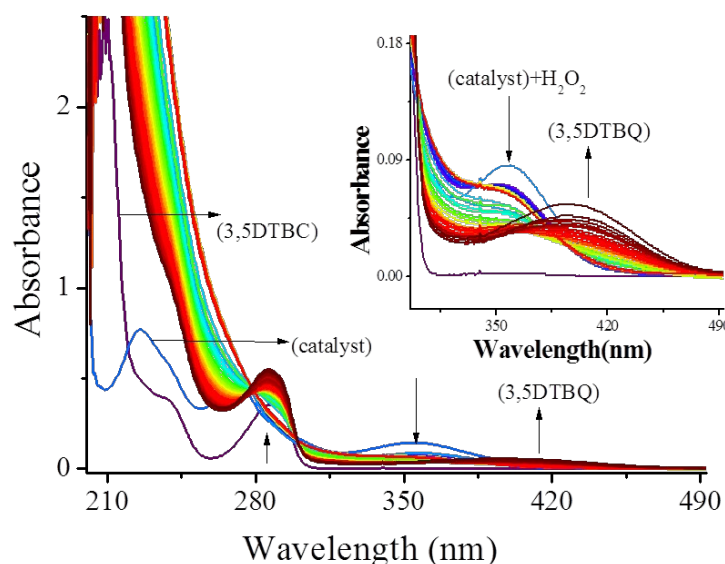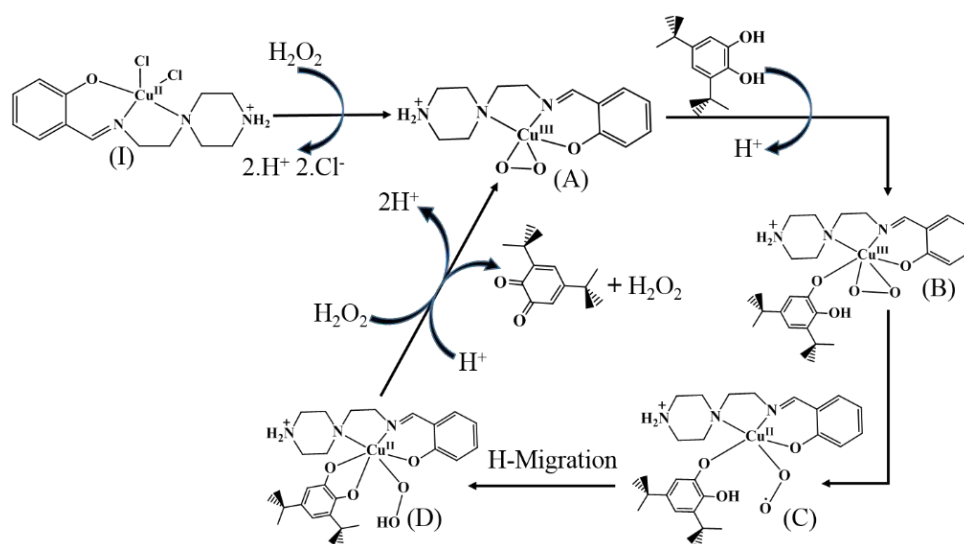
Figure 16: Spectral changes observed during the progressive addition of 1 drop portion of 6.0×10^{-2} M methanolic solution of 3,5-DTBC into 20 ml methanolic solution of $[Cu^{III}(O_2)(hyap\text{-}ppzH)]$. Spectra were recorded at room temperature with 3 min of time interval. Insert shows the expanded view of the same spectral change in the 300-490 nm region.


Scheme 5: Proposed mechanism for the oxidation of 3,5-DTBC by the complex **1**, at room temperature and pressure in the presence of dilute H_2O_2 based on the UV-Vis spectroscopic, pH measurement and ESI-MS analysis.

Among the two catalysts, efficiency trends for the oxidation of 3,5-DTBC,follow as [Cu^{II}(hyap-ppzH)Cl_2] (**2**)>[Cu^{II}(sal-ppzH)Cl_2] (**1**). Because of the complicated nature of the actual reaction mechanism, it is very difficult to rationalize the actual reason for the enhanced reactivity of the reported complexes. But based on the UV-Vis spectrophotometric studies and ESI-MS analysis we can conclude that switching between [Cu^{II}(HL)Cl_2] and η^2-side on peroxo [Cu^{III}(O_2)(L)] is necessary step during the catalytic cycle. However, maintaining the stability for both of the redox states, flexible coordinating environment is required. For that, mononuclear non-planer complex with trigonal bi-pyramidal, square pyramidal geometry or slightly distorted geometry is more favorable than a rigid square planar geometry. Additional enhancement in the catalytic activity can be observed if metal complexes possess accessible labile ligands site (s) for the substrate binding. Both the reported copper complexes possess slightly distorted square pyramidal geometry along with two labile ligand (Cl) sites which makes them suitable candidates for the easy oxidation of 3,5-DTBC. DFT calculation also shows that the EA (electron affinity) of [Cu^{II}(hyap-ppzH)Cl_2] (**2**) and [Cu^{II}(sal-ppzH)Cl_2] (**1**) are -79.09 Kcal/mole and -76.37 Kcal/mole respectively (table 6). While IP (Ionization Potential) of **2**(-133.19 kcal/mole) is comparatively smaller than the complex **1** (-134.73 Kcal/Mole), explains the easy oxidation of **2** to the corresponding η^2-side on peroxo complex which is the active species for the catalytic oxidation of 3,5-DTBC to the corresponding 3,5-DTBQ. Although both complexes quite efficiently oxidize3,5-DTBC, but because of easily available active peroxo species of **2** in solution makes it little more efficient than **1** (table 7)**.**

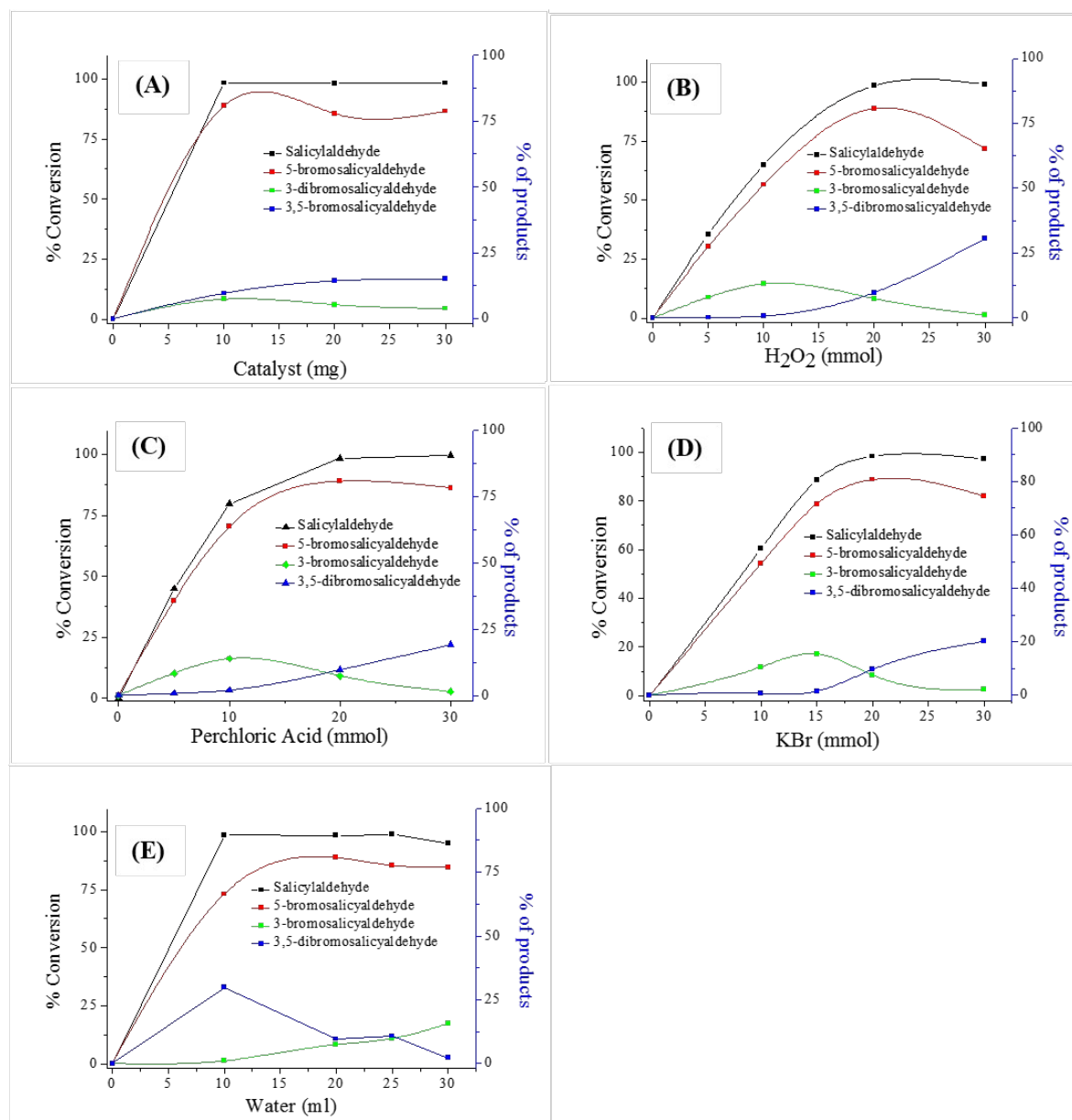### 3.10.2. *Oxidative bromination of Salicylaldehyde*

Oxidative bromination of salicylaldehyde was carried out by using polymer anchored copper(II) complexes as catalyst precursors. Three major oxidative bromination products i.e. 5-bromo-2-hydroxybenzaldehyde,   3-bromo-2-hydroxybenzaldehyde   and   3,5-dibromo-2-hydroxybenzaldehyde were identified during the catalytic reaction (scheme 6). The maximum conversion was obtained by optimized various reaction parameters namely amount of catalyst, amount of oxidant (30 % aqueous H_2O_2), amount of perchloric acid, amount of potassium bromide and amount of solvent. PS-[Cu^{II}(sal-ppz)Cl] (**3**) was used as a representative catalyst while keeping other reaction conditions such as RPM of magnetic stirrer, size of magnetic bead, shape and size of reaction flask etc. as identical as possible. In the oxidative bromination, half of the perchloric acid was added at the beginning of the reaction (t=0 min) and rest of the amount was

added to the reaction mixture in three equal portions at a fixed time interval (after every 15 min). In all cases prior to the reaction, polymer anchored catalysts were swelled in water for 6 hours.
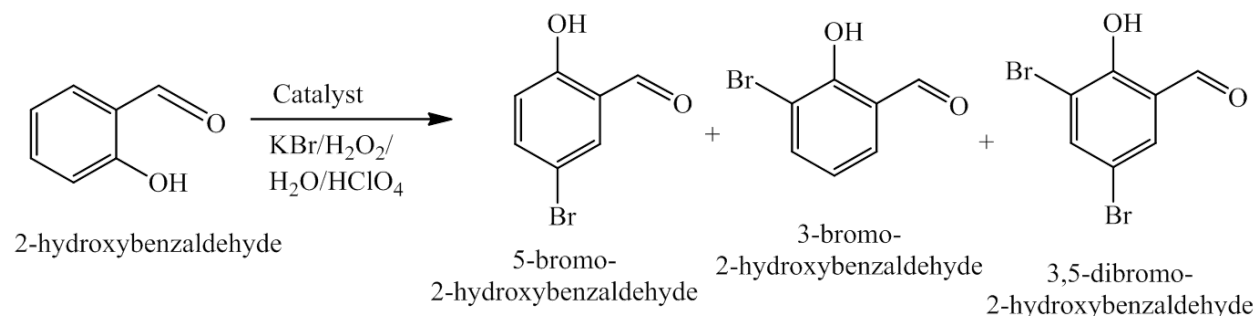
Scheme 6: Major oxidative bromination products of Salicylaldehyde.

To optimize the amount of catalyst for the oxidative bromination of salicylaldehyde, three different amounts of pre-swelled catalysts (0.010 g, 0.020 g and 0.030 g) were taken while reacting 10 mmol (1.22 g) of salicylaldehyde with 20 mmol (2.38 g) KBr, 20 mmol (2.86 g) $HClO_4$ and 20 mmol (2.26 g) 30% H_2O_2 in 20 ml water under smooth stirring (800 RPM) at room temperature and pressure for 2 hours. The effect of amount of catalyst on the oxidative bromination of salicylaldehyde is displayed in plot 3-A. It is evident from the plot 3-A that 0.010 g catalyst gives 98.36 % product conversion with the formation of 5-bromosalicylaldehyde (80.70%) as major product. The % of products formed by using catalyst **3** follows the order 5-bromosalicylaldehyde(80.70%)>3,5-dibromosalicylaldehyde(9.60%)>3-bromosalicylaldehyde (7.41 %). While catalyst amount 0.020 g and 0.030 g shows nearly the similar % conversion i.e. 98.23% and 98.36% respectively.

New Journal of Chemistry Accepted Manuscript

Plot 3: Plot of % conversion and % of product formation against the various reaction parameters of the oxidative bromination of salicylaldehyde at room temperature and pressure. (A) Impact of amount of catalyst; (B) Impact of 30% aqueous H_2O_2; (C) Impact of amount of 70% aqueous perchloric acid; (D) Effect of amount of potassium bromide and (E) Effect of volume of solvent (H_2O). Reaction conditions for plot (A), (B), (C), (D) and (E) are mentioned in the text.

Therefore an amount of 0.010 g of catalyst **3** was set as optimum. The impact of amount of H_2O_2 was studied by changing the substrate to oxidant ratio of 2:1, 1:1, 1:2 and 1:3 for a fixed amount of salicylaldehyde (1.22 g,10 mmol), pre-swelled catalyst precursor (0.010 g), KBr (2.38

g, 20 mmol) and $HClO_4$(2.86 g, 20 mmol) in 20 ml water under stirring (RPM 800) at room temperature and pressure for 2 hours (plot 3-B). Plot 3-B shows that % conversion increases from 35.35% to 64.96% with increasing the substrate to oxidant ratio from 2:1 to 1:1 and a 1:3 ratio is enough to achieve the 98.38% conversion of salicylaldehyde. Further increasing the ratio does not improve the % conversion, only the change in % products formation observed, i.e. 1:2 ratio shows, 80.70% 5-bromosalicylaldehyde, 9.60% 3,5-dibromosalicylaldehydeand 7.41% 3-bromosalicylaldehydewhile 1:3 ratio gives 65.09% 5-bromosalicylaldehyde, 30.45% 3,5-dibromosalicylaldehyde and 0.89% 3-bromosalicylaldehyde (table 8).

Table 8: Data for the oxidative bromination of salicylaldehyde catalyzed by the catalyst **3** and **4.** % conversion, TOF and % of products obtained after 2 hours of reaction at room temperature and pressure**.**

S N	Cat. Precursor	catalyst (mg)	Substrate :Oxidant	$HClO_4$ (mmol)	Water (ml)	KBr (mmol)	Conversion %	TOF /h	% of products			
									5-bromosalicylaldehyde	3-bromosalicylaldehyde	3,5-dibromosalicylaldehyde	Unidentified pdts
1	**3**	10	1:2	20	20	20	98.38	3.98×10^4	80.70	7.41	9.60	0.67
2	**3**	20	1:2	20	20	20	98.23	1.99×10^4	77.79	5.34	14.31	0.79
3	**3**	30	1:2	20	20	20	98.36	1.32×10^4	78.68	3.85	15.13	0.7
4	**3**	10	2:1	20	20	20	35.35	1.43×10^4	27.40	7.83	0.094	0.026
5	**3**	10	1:1	20	20	20	64.96	2.63×10^4	51.25	13.04	0.612	0.058
6	**3**	10	1:3	20	20	20	98.91	4.01×10^4	65.09	0.89	30.45	2.48
7	**3**	10	1:2	5	20	20	44.88	1.81×10^4	35.72	8.35	0.78	0.03
8	**3**	10	1:2	10	20	20	79.65	3.22×10^4	63.54	13.85	2.00	0.26
9	**3**	10	1:2	30	20	20	99.45	4.03×10^4	78.14	1.45	19.10	0.76
10	**3**	10	1:2	20	20	10	60.53	2.45×10^4	49.34	10.55	0.63	0.01
11	**3**	10	1:2	20	20	15	88.54	3.58×10^4	71.61	15.44	1.40	0.09
12	**3**	10	1:2	20	20	30	97.26	3.94×10^4	74.46	2.13	20.09	0.58
13	**3**	10	1:2	20	10	20	98.47	3.99×10^4	66.44	1.02	29.89	1.12
14	**3**	10	1:2	20	25	20	98.83	4.00×10^4	77.66	9.77	10.84	0.56
15	**3**	10	1:2	20	30	20	94.95	3.84×10^4	76.86	15.69	2.15	0.25
16	**4**	10	1:2	20	10	20	94.40	7.51×10^3	68.56	1.64	23.07	0.834
17	**1**	0.0453	1:2	20	10	20	91.19	3.69×10^4	55.20	4.50	29.74	1.73
18	**2**	0.239	1:2	20	10	20	96.85	7.71×10^3	62.79	3.83	28.56	1.65

New Journal of Chemistry Accepted Manuscript

The effect of $HClO_4$, added as an aqueous 70% $HClO_4$ solution, was examined by taking four different amounts, 5 mmol (0.715 g), 10 mmol (1.43 g), 20 mmol (2.86 g) and 30 mmol (4.29 g) for fixed amount of salicylaldehyde (1.22 g,10 mmol), pre-swelled catalyst precursor (0.010 g),20 mmol (2.26 g) 30 % H_2O_2 and KBr (2.38 g, 20 mmol) in 20 ml water under stirring (RPM 800) at room temperature and pressure for 2 hours (plot 3-C).By increasing the perchloric acid amount from 5 mmol (0.715 g) to 10 mmol (1.43 g), significant improvement in the % conversion from 44.88% to 79.65% was observed. With increasing the amount of perchloric acid amount from 10 mmol (1.43 g) to 20 mmol (2.86 g), % conversion continues to increases from 79.65% to 98.38%. But 30 mmol (4.29 g)$HClO_4$gives only a marginal increment in the % conversion (99.45%). So 20 mmol (2.86 g) $HClO_4$ was considered as optimum. Addition of $HClO_4$ in four equal portions during the reaction was necessary to improve the % conversion and keep away the decomposition of catalyst. Most of the catalytic reaction proceeds with slow decomposition of catalyst. Addition of $HClO_4$ with a constant time interval can reduce the catalyst decomposition[115].
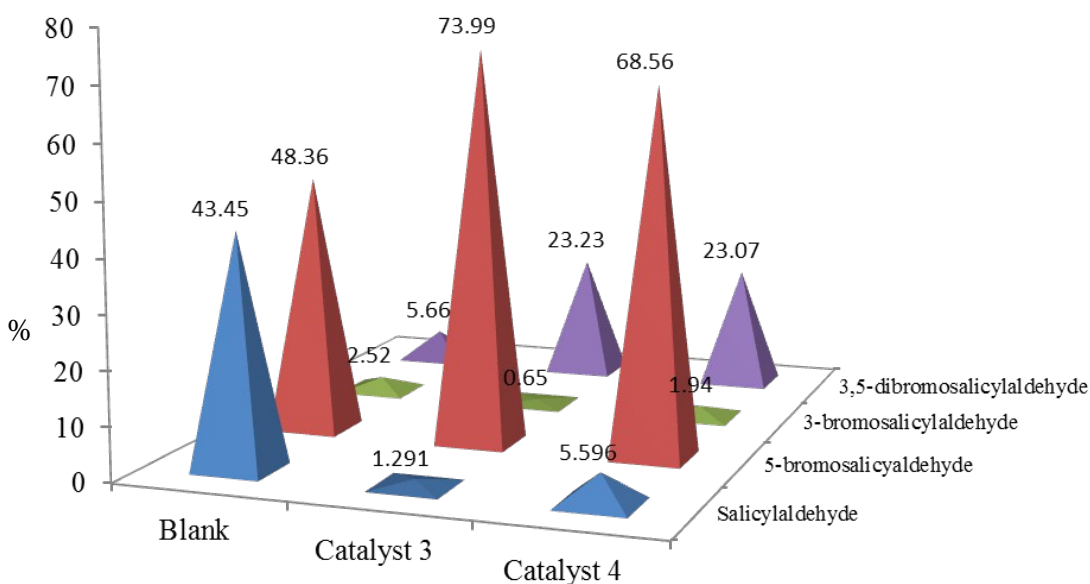
Plot 4: Impact of catalysts: % of salicylaldehyde remain and % of products formed by Blank reaction, **3** and **4** in the oxidation bromination of salicylaldehyde at room temperature and pressure for 2 hours.

The amount of KBr also affects the % conversion as well as the % of product formation on the oxidative bromination of salicylaldehyde. In search of the optimum amount of KBr, four different amounts of KBr, 10 mmol (1.19 g), 15 mmol (1.78 g), 20 mmol (2.38 g) and 30 mmol (3.57 g) were used for a fixed amount of salicylaldehyde (1.22 g ,10 mmol), pre-swelled catalyst precursor (0.010 g),20 mmol (2.26 g) 30% H_2O_2 and $HClO_4$ (2.86 g, 20 mmol) in 20 ml water under stirring (RPM 800) at room temperature and pressure for 2 hours (plot 3-D). Plot 3-D shows that the substrate : KBr ratio 1:1 gives 60.53% conversion while 2:3 and 1:2 ratio produce 88.54% and 98.38% conversion respectively. Further increasing the KBr amount does not increase the % conversion, only changes the order of % products formation (Table 8). 1:2 ratio gives, 80.70% 5-bromosalicylaldehyde, 9.60% 3,5-dibromosalicylaldehydeand and 7.41% 3-bromosalicylaldehydewhile, 1:3 ratio gives74.46% 5-bromosalicylaldehyde, 20.09% 3,5-dibromosalicylaldehydeand 2.13% 3-bromosalicylaldehyde (table 8). Thus an amount of 20 mmol (2.38 g) of KBr (substrate: KBr, 1:2) was set as optimum.

Similarly four different amounts of solvent (water) were used for the oxidative bromination of salicylaldehyde. It is evident from the plot 3-E that 10 ml, 20 ml and 25 ml of solvent (water) produces approximately similar % conversion (98.47%, 98.38%, and 98.83% respectively) with similar trends in their % of products formation i.e.5-bromosalicylaldehyde>3,5-dibromosalicylaldehyde>3-bromosalicylaldehyde. With further increasing the amount of solvent % conversion reduces slightly (table 8); may be because of less effective collision among the reactant molecules in a much dilute solution.

Finally in the table 8, SL. No. 13 represents the fully optimized reaction conditions for the oxidative bromination of salicylaldehyde at room temperature and pressure by **3,** which are 10 mmol (1.22 g) salicylaldehyde, 0.010 g pre-swelled catalyst precursor, 20 mmol (2.26 g) 30 % $H_2O_2,$ 20 mmol (2.86 g)$HClO_4$, 20 mmol (2.38 g) KBr, 10 ml of water and 2 hours of time. Under the optimized reaction condition **3** shows 98.47 % conversion with TOF value 3.99×10^4. By the consumption of salicylaldehyde in optimized condition,**3**givesthree major products namely 5-bromosalicylaldehyde (66.44%), 3,5-dibromosalicylaldehyde (29.89%), and 3-bromosalicylaldehyde (1.02%) along with a very small % of 1,3,5 tribromo phenol. It should be noted that optimized conditions were set for the maximum conversion of salicylaldehyde and 5-bromosalicylaldehyde was isolated as a major product amongst the three.

Catalytic activity of the complex PS-[Cu(hyap-ppz)Cl](**4**) was also tested under the above mentioned optimized condition. Catalyst **4** exhibit 94.40% conversion with TOF value 7.51×10^3 in the optimized condition. **4** shows very similar products distribution to that of catalyst **3**. Because of similar electronic environment both catalysts show close resemblance. However, catalyst **3** is little more efficient in comparison to catalyst **4**.

A blank reaction under the same optimized condition shows only 56.55 % conversion (plot 4).Also by using $CuCl_2.2H_2O$ as a catalyst under the identical optimized condition, salicylaldehyde show only 84.61 % conversion (table S4). Salicylaldehyde show less than 3% of normal oxidation reaction without KBr under the optimized reaction condition, which indicates its stability and eliminates parallel oxidation of salicylaldehyde during oxidative bromination. Neat complexes **1** and **2** also catalyzed the oxidative bromination of salicylaldehyde and shows 91.19% and 96.85 % conversion respectively. Activity of the neat complexes **1** and **2**might be close to that of polymer anchored complexes **3** and **4,** but greater stability, easy separation from the reaction mixture, and recyclability makes the polymer anchored metal complexes better choice over the neat complexes. Vanadium bromoperoxidase, a vanadium containing metalloenzyme responsible for the oxidation of bromide ion and if suitable organic substrate is present, brominates the organic molecules otherwise react with another molecule of $Br^-$to form bromine. Based on vanadium bromoperoxidase model a number of attempts were made to establish the reaction mechanism of oxidative bromination of organic substrates, by combining reactivity analysis along with spectroscopic and theoretical studies.[116, 117-119, 61]

In present study, similar vanadium bromoperoxidase activity is exhibited by **3** and **4,** in spite of the fact that vanadium bromoperoxidase contains vanadium in the active site while we examined the complexes of copper. On the basis of the reactivity studies ESI-MS, and spectroscopic measurements, it can be concluded that the reaction proceeds as reported in the literature. In brief, copper(II) complexes form η^2-side on peroxo Cu^{3+} complex $[Cu^{III}(O_2)(L)]$ by reacting with aqueous hydrogen peroxide, that oxidizes bromide ion (from aqueous KBr) into bromine equivalent intermediate. Generated active bromine intermediate then either reacts with salicylaldehyde and bromination products form or reacts with another active bromine intermediate and generates bromine. Copper(II) catalyst acts as a Lewis acid and creates a more strong oxidizing agent (metal peroxide) than hydrogen peroxide.

3.9.2.1. *Test for recycle ability*

The recycle ability of polymer grafted complexes PS-[Cu(sal-ppz)Cl] (**3**) and PS-[Cu(hyap-ppz)Cl] (**4**) have been checked. After 2 hours of oxidative bromination, catalysts were filtered and washed with water followed by methanol and dried in hot oven at 120°C for 24 hours. Properly dried catalysts were used in the oxidative bromination under similar reaction conditions. After one cycle catalysts **3** and **4** show 96.16 % and 91.14 % conversion respectively. After two cycles, catalysts **3** and **4** show 88.76 % and 86.46 % conversion. Close % conversion with respect to fresh catalysts, indicates their easy recycle ability. With increasing number of catalytic cycle, probability of metal leaching increases. Little difference in the % conversion between fresh and used catalyst is a measure of extent of metal leaching.

4. Conclusions

We have successfully synthesized two new copper(II) complexes containing schiff-base ligands [Hsal-ppz] (**I**) and[Hyap-ppz] (**II**) derived from the reaction of 1-(2-Aminoethyl) piperazine with salicylaldehyde and 2-hydroxyacetophenone respectively. The complexes are monomeric in nature both in solid state and in solution. Both of these complexes are also anchored on to the polymeric matrix of chloromethylated polystyrene. All the ligands and metal complexes were characterized by various analytical and spectroscopic techniques. Structure of the complex [Cu^{II}(sal-ppzH)Cl_2] (**1**),was confirmed by single crystal XRD studies. DFT calculation suggests similar molecular structure for the complex **2**.

Catalytic activity for the oxidation of 3,5-DTBC to the corresponding 3,5-DTBQ was evaluated by **1**and **2**. **1** and **2**shows enhanced catalytic activity with high turnover number 1.182×10^4 mmolh^{-1} and 2.880×10^4 mmolh^{-1} respectively. Oxidation of the 3,5-DTBC proceeds through reactive intermediate η^2-side on peroxo [Cu^{III}(O_2)(L)] complex which has been established from pH metric titration, electronic absorption spectroscopy and ESI-MS analysis.

Polymer anchored copper(II) complexes PS-[Cu(sal-ppz)Cl](**3**) and PS-[Cu(hyap-ppz)Cl](**4**) act as functional models of vanadium bromoperoxidase and successfully catalyze the oxidative bromination of salicylaldehyde. Under optimized reaction condition **3** shows 98.47% conversion with the order of % products formed:5-bromosalicylaldehyde>3,5-dibromosalicylaldehyde>3-bromosalicylaldehyde. While **4** shows 94.40% conversion with similar order of % products distribution. The corresponding neat complexes **1** and **2** also shows close catalytic activity. Recyclability and easy separation from the reaction mixture makes polymer bound catalysts better

choice in comparison to their neat one. No significant loss in their catalytic activity was observed at least up to two cycles. Under the specified reaction condition **2** is more efficient than **1** for the oxidation of 3,5-DTBC, while **3** is better in comparison to **4** for the oxidative bromination of salicylaldehyde.

Supporting information's

Tables containing single crystal XRD, bond length and bond angle for **1,** FTIR and UV-Vis data and figures for the ligands, complexes and polymer anchored metal complexes, ^{1}H NMR and ^{13}C NMR spectra of the ligands, Cyclic Voltagram of complex **1** and ESI-MS data for the peroxo copper complexes, are submitted as supporting materials.

Conflicts of interest

There are no conflicts of interest to declare

Acknowledgements

References

1. E. Tsuchida, K. Oyaizu, Coord. Chem. Rev., 2003,**237**,213.
2. L. Canali, D. C. Sherrington, Chem. Soc. Rev., 1999,**28,** 85.
3. J. Tisato, F. Refosco, F. Bandoli, Coord. Chem. Rev., 1994, **135,** 325.

4. M. K. Islam, T. Miyoshi, M. Yamada, M. A. Alim, X. Huang, M. Motobu, N. Tsuji, Acta. Trop., 2006,**99**, 208.

5. P. Chaudhary, R. Kumar, A. K. Verma, D. Singh, V. Yadav, A. K. Chhillar, G. L. Sharma, R. Chandra, Bioorgan. Med. Chem., 2006,**14**, 1819.

6. S. C. J. N. Narendra, C. T. Sadashiva, C. V. Kavitha, K. S. Rangappa, Bioorg. Med. Chem.,2006,**14,**6621.

7. C. T. Sadashiva, Narendra, S. C. J. N., K. C. Ponnappa, G. T. Veerabasappa, K. S. Rangappa, Bioorgan. Med. Chem. Lett., 2006,**16,**3932.

8. D. Nozawa, T. Okubo, T. Ishii, K. Takamor, S. Chaki, S. Okuyama, A. Nakazato, Bioorg. Med. Chem., 2007, **15**, 2375.

9. C. Chen, W. Jiang, F.TucciJ, A. Tran, B. A. Fleck, S. R. Hoare, M. Joppa, S. Markison, J. Wen, C. W. Chen, J.Med. Chem., 2007,**50**, 5249.

10. R. F. Staack, L. D. Paul, D. Springer, T. Kraemer, H. H. Maurer, Biochem. Pharmacol.,2004, **67,**235.

11. N. Serradji, O. Bensaid, M. Martin, W. Sallem, N. D. Bosquet, H. Benmehdi, Redeuilh, C. Lamouri, A. Dive, G. P. Clayette, Bioorg. Med. Chem., 2006,**14,**8109.

12. H. Benmehdi, A. Lamouri, N. Serradji, F. Pallois, F. Heymans, Eur. J. Org. Chem., 2008, 299.

13. W. Allem, N. Serradji, N. D. Bosquet, G. Dive, P. Clayette, F. Heymans, Bioorg. Med. Chem., 2006, **14**, 7999.

14. M. S. Salga, H. M. Ali, M. A. Abdullah, S. I. Abdelwahab, P. D. Hussain, A. H. AHadi, Molecules., 2011, **16,**8654.

15. M. Yu, M. Lizarzaburu, H. Beckmann, R. Connors, K. Dai, K. Haller, C. L. Liang, L. M. Lindstrom, J. Ma, Bioorg. Med. Chem. Lett., 2010,**20,**1758.

16. S. Y. Seo, V. K. Sharma, N. Sharma, M. Tyrosinase, Recent Prospects. J. Agric. Food Chem., 2003,**51**,2837.

17. R.Yoruk, M. R. Marshall, J. Food Biochem., 2003,**27**,361.

18. F. Artes, M. Castaner, M. I. Gil, Food Sci. Technol. Int.,1998,**4**,377.

19. C. Fernandes, A. Neves, A. J. Bortoluzzi, A. S. Mangrich, E. Rentschler, B. Szpoganicz, E. Schwingel, Inorg. Chim. Acta.,2001,**320**,12.

20. E. Moura, J. Afonso, L. Hein, M. A. Vieira-Coelho, Br. J. Pharmacol., 2006,**149**,1049.

21. B. J. Deverall, Nature.,1961,**189**, 311.

22. S. K. Dey, A. Mukherjee, Coordination Chemistry Reviews.,2016,**310**,18.

23. K. Selmeczi, M. Réglier, M. Giorgi, G. Speier, Coord. Chem. Rev., 2003,**245**,191.

24. H. Börzel, P. Comba, H. Pritzkow, Chem. Commun., 2001,**97**, 97.

25. E. Monzani, G. Battaini, A. Perotti, L. Casella, M. Gullotti, L. Santagostini, G. Nardin, L. Randaccio, S. Geremia, P. Zanello, G. Opromolla, Inorg. Chem.,1999, **38**,5359.

26. E. Monzani, L. Quinti, A. Perotti, L. Casella, M. Gullotti, L. Randaccio, S. Geremia,G. Nardin, P. Faleschini, G. Tabbi, Inorg. Chem., 1998,**37**,553.

27. G. Grigoropoulou, K. C. Christoforidis, M. Louloudi, Y. Deligiannakis, Langmuir, 2007, **23**,10407.

28. G. Speier, J. Mol. Catal., 1986,**37**,259.

29. Z. F. Chen, Z. R. Liao, D. F. Li, W. K. Li, X. G. Meng, J. Inorg. Biochem.,2004,**98**,1315.

30. D. Dey, A. B. Roy, A. Ranjani, L. Gayathri, S. Chandraleka, D. Dhanasekaran, M. A. Akbarsha, C. Y. Shen, H. L. Tsai, M. Maji, N. Kole, B. Biswas, J. Chem. Sci., 2015, **127**,649.

31. L. Mandal, S. Sasmal, H. A. Sparkes, J. A. K. Howard, S. Mohanta, Inorg. Chim. Acta.,2014, **412**,38.

32. R. Modak, Y. Sikdar, S. Mandal, S. Goswami, Inorg.Chem. Commun., 2013,**37,** 193.

33. S. Majumder, S. Mondal, P. Lemoine, S. Mohanta, Dalton Trans., 2013,**42**, 4561.

34. A. Banerjee, A. Guha, J. Adhikary, A. Khan, K. Manna, S. Dey, E. Zangrando, D. Das, Polyhedron., 2013,**60**,102.

35. K.S. Banu, T. Chattopadhyay, A. Banerjee, M. Mukherjee, S. Bhattacharya, G. K. Patra, E. Zangrando, D. Das, Dalton Trans., 2009, 8755.

36. S. K. Dey, A. Mukherjee, ChemCatChem.,2013,**5**,3533.

37. A. Guha, K. S. Banu, A. Banerjee, T. Ghosh, S. Bhattacharya, E. Zangrando, D. Das, J. Mol. Catal. A: Chem., 2011,**338**,51.

38. M. Pait, M. Shatruk, D. Ray, Dalton Trans.,2015,**44**,11741.

39. A. Banerjee, A. Guha, P. Maiti, S. Goswami, T. Chattopadhyay, T. K. Mondal, S. Bhattacharya, E. Zangrando, D. Das, Transition Met. Chem.,2011,**36**,829.

40. R. Modak, Y. Sikdar, S. Mandal, S. Chatterjee, A. Bienko, J. Mrozinski, S. Goswami, Inorg. Chim. Acta., 2014,**416**,122.

41. M. Das, R. Nasani, M. Saha, S. M. Mobin, S. Mukhopadhyay, Dalton Trans., 2015,**44**,2299.

42. S. Das, P. Maiti, T. Ghosh, E. Zangrando, D. Das, Inorg. Chem. Commun.,2012,**15**,266.

43. A. Guha, T. Chattopadhyay, N.D. Paul, M. Mukherjee, S. Goswami, T.K. Mondal, E. Zangrando, D. Das, Inorg. Chem., 2012,**51**,8750.

44. D. Dey, G. Kaur, A. Ranjani, L. Gayathri, P. Chakraborty, J. Adhikary, J. Pasan, D. Dhanasekaran, A. R. Choudhury, M. A. Akbarsha, N. Kole, B.Biswas, Eur. J. Inorg. Chem., 2014, 3350.

45. M. Mitra, A.K. Maji, B. K. Ghosh, P. Raghavaiah, J. Ribas, R. Ghosh, Polyhedron., 2014,**67**,19.

46. P. Comba, H. Wadepohl, S. Wunderlich, Eur. J. Inorg. Chem., 2011, 5242.

47. U. Russo, M. Vidali, B. Zarli, R. Purrello, G. Maccarrone, Inorg. Chim. Acta.,1986,**120**,11.

48. S. I. Lo, J.W. Lu, W.J. Chen, S.R. Wang, H.H. Wei, M. Katada, Inorg. Chim. Acta., 2009,**362**,4699.

49. S. K. Mal, M. Mitra, B. Biswas, G. Kaur, P. P. Bag, C. M. Reddy, A. R. Choudhury, N. A. Alcalde, R. Ghosh, Inorg. Chim. Acta., 2015,**425**,61.

50. C. Bianchini, P. Barbaro, V. Dal Santo, R. Gobetto, A. Meli, W. Oberhauser, R. Psaro, F. Vizza, Adv. Synth Catal., 2001,**343**,41.

51. N.B. Barhate, A.S. Gajare, R.D. Wakharkar, A.V. Badekar, Tetrahedron Lett.,1998,**39**,6349.

52. R. Neumann, I. Assael, J. Chem. Soc. Chem. Commun., 1988, 1285.

53. C. R. Cornman, J. Kampf, V. L. Pecoraro, Inorg. Chem., 1992,**31**,1981.

54. C. R. Cornman, J. Kampf, M. S. Lah, V. L. Pecoraro, Inorg. Chem., 1992,**31**,2035.

55. C. R. Cornman, G. J. Colpas, J. D. Hoeschele, J. Kampf, V. L. Pecoraro, J. Am. Chem. Soc., 1992,**114**,9925.

56. M. R. Maurya, A. Kumar, M. Ebel, D. Rehder, Inorg. Chem., 2006,**45**,5924.

57. L. J. Calviou, J. M. Arber, D. Collison, C. D. Garner, W. Clegg, J. Chem. Soc., Chem. Commun., 1992, 654.

58. A. D. Keramidas, S. M. Miller, O. P. Anderson, D. C.Crans, J. Am. Chem. Soc., 1997, **119**,8901.

59. V. Conte, F. di Furia, S. Maro, Tetrahedron Lett., 1994,**45**,7429.

60. M.R. Maurya, S. Sikarwar, T. Joseph, P. Manikandan, S.B. Halligudi, React. Funct. Polym.,2005,**63**,71.

61. M. R. Maurya, C. Haldar, A. Kumar, B. Maxim L. Kuznetsov, B. F. Avecillac, J. C. Pessoa, Dalton Transactions, 2013,**42**,11941.

62. N. Narender, K.V.V.K. Mohan, R.V. Reddy, P. Srinivasu, S.J. Kulkarni, K.V. Raghavan, J. Mol. Catal. A: Chem., 2003,**192**,73.

63. Sk. M. Islam, P. Mondal, A. S. Roy, N. Salam, S. Paul, Catal. Lett., 2013,**143,**225.

64. S. M. Islam, A. S. Roy, P. Mondal, K. Tuhina, M. Mobarak, J. Mondal, Tetrahedron Letters, 2012,**53**,127.

65. N. Oishi, Y. Nishida, K. Ida, S. Kida, Bull. Chem. Soc. Jpn., 1980,**53**,2847.

66. S. Mukhopadhyay, D. Mandal, D. Ghosh, I. Goldberg, M. Chaudhury, Inorganic Chemistry, 2003,**42**, 25,8439.

67. M. S. Salga, H. Khaledi, H. M. Ali, ActaCryst.,2010. E66, m1131. S/cat 1:2000-1:200.

68. R. L. Dotson, Inorg. nucl. chem.,1974,**10,**879.

69. APEX2 - Software Suite for Crystallographic Programs, Bruker AXS, Inc.: Madison, WI, USA, 2009.

70. G. M. Sheldrick, ActaCryst. C., 2015,**71**,3.

71. L. J. Farrugia, J. Appl. Cryst.,2012,**45**,849.

72. G. M. Sheldrick, SADABS-2008/1 - Bruker AXS area detector scaling and absorption correction, Bruker AXS: Madison, Wisconsin, USA, 2008.

73. A. L. Spek, PLATON, A Multipurpose Crystallographic Tool, 1.17; Utrecht University: Utrecht, The Netherlands, 2011.

74. M. J. Frisch, GAUSSIAN 09, Rev. D.01, Gaussian, Inc., Wallingford, CT, 2009.

75. R. D. Dennington II, T. A. Keith, J. M. Millam, GaussView 5.0, Wallingford, CT, 2009.

76. http://www.chemcraftprog.com

77. A. D. Becke, J. Chem. Phys., 1993,**98**,5648.

78. C. Lee, W. Yang, R.G. Parr, Phys. Rev. B., 1988,**37**,785.

79. B. D. Becke, Phys. Rev. B., 1988,**38**,3098.

80. S. H. Vosko, L. Wilk, M. Nusair, Can. J. Phys., 1980,**58**,1200.

81. J. Ravichandran, P. Gurumoorthy,C. Karthick, A. K. Rahiman, Journal of Molecular Structure, 2014,**1062**,147.

82. M. J. Gajewska, W. M. Ching, Y. S. Wen, C. H. Hung, Dalton Trans., 2014,**43**,14726.

83. X. Das, K. Sinha, C. Datta, A. Garribba, E. Fondo, M. Mautner, F.A. Fischer, R.C. J. Chem. Res, 2012, **36**, 12, 722*.*

84. Y. C. Urquiola, D. Gambino, M. Cabrera, M. L. Lavaggi, H. Cerecetto, M. Gonza´lez, A. L.´pez de Cerain, A. Monge, A. J. Costa-Filho, M. H. Torre, Journal of Inorganic Biochemistry, 2008, **102**, 119.

85. I. Mohamed, Orifand H. Mohamed, A. Rhman, doi.org/10.1016/j.poly.2015.06.021

86. K. Fukui, Science, 1982, **218**, 4574, 747.

87. C. A. Alvar, M. S. Soylu, A. Güder, Ç. D. Albayrak, G. Apaydin, N. Dilek, SpectrochimicaActa Part A: Molecular and Biomolecular Spectroscopy, 2014,**125**,319.

88. F. Zippel, F. Ahlers, R. Werner, W. Haase, H. F. Nolting, B. Krebs, Inorg. Chem., 1996, **35**,3409.

89. A. Neves, L. M. Rossi, A. J. Bortoluzzi, A. S. Mangrich, W. Haase and R. Werner, J. Braz. Chem. Soc., 2001,**12**,6,747.

90. J. Reim, B. J. Krebs, J. Chem. Soc., Dalton Trans., 1997, 3793.

91. J. Reim, R. Werner, W. Hasse, B. Krebs, Chem. Eur. J., 1998,**4**,289.

92. A. Neves, L. M. Rossi, A. J. Bortoluzzi, A. S. Mangrich, W. Haase, R. J. Werner, Braz. Chem. Soc., 2001,**12**,747.

93. A. Neves, L. M. Rossi, A. J. Bortoluzzi, B. Szpoganicz, C. Wiezbicki, E. Schwingel, W. Haase, S. Ostrovsky, Inorg. Chem., 2002,**41**,1788.

94. F. Zippel, F. Ahlers, R. Werner, W. Haase, H. F. Nolting, B. Krebs, Inorg. Chem., 1996,**35**,3409.

95. E. Monzani, L. Quinti, A. Perotti, L. Casella, M. Gullotti, L. Randaccio, S. Geremia, G. Nardin, P. Faleschini, G. Tabbi, Inorg. Chem., 1998,**37**,553.

96. P. Gentschev, N. Möller, B. Krebs, Inorg. Chim. Acta., 2000,**300**,442.

97. C. T. Yang, M. Vetrichelvan, X. Yang, B. Moubaraki, K.S. Murray, J.J. Vittal, Dalton Trans., 2004, 113.

98. X. Wang, J. Ding, J.J. Vittal, Inorg. Chim. Acta., 2006,**359**,3481.

99. I. A. Koval, P. Gamez, C. Belle, K. Selmeczi, J. Reedijk, Chem. Soc. Rev., 2006,**35**,814.

100. I. A. Koval, C. Belle, K. Selmeczi, C. Philouze, E. Saint-Aman, A. M. Schuitema, P. Gamez, J. L. Pierre, J. Reedijk, J. Biol. Inorg. Chem., 2005,**10**,739.

101. R. E. H. M. B. Osorio, R. A. Peralta, A. J. Bortoluzzi, V. R. de Almeida, B. Szpoganicz, F. L. Fischer, H. Terenzi, A. S. Mangrich, K. M. Mantovani, D. E. C. Ferreira, W. R. Rocha, W. Haase, Z. Tomkowicz, A. dos Anjos, A. Neves, Inorg. Chem., 2012,**51**, 1569.

102.   I. A. Koval, K. Selmeczi, C. Belle, C. Philouze, E. Saint-Aman, I. G. Luneau, A. M. Schuitema, M. van Vliet, P. Gamez, O. Roubeau, M. Lueken, B. Krebs, M. Lutz, A. L. Spek, J. L. Pierre, J. Reedijk, Chem. Eur. J., 2006,**12**,6138.

103. J. Ackermann, F. Meyer, E. Kaifer, H. Pritzkow, Chem.Eur. J., 2002,**8**,247.

104. M. Kodera, T. Kawata, K. Kano, Y. Tachi, S. Itoh, S. Kojo, Bull. Chem. Soc. Jpn., 2003,**76**,1957.

105. J. Kaizer, J. Pap, G. Speier, L. Parkanyi, L. Korecz, A. Rockenbauer, J. Inorg. Biochem.,2002,**91**,190.

106. G. Speier, New J. Chem., 1994,**18**,143.

107. J. Adhikary, P. Chakraborty, S. Das, T. Chattopadhyay, A. Bauza, S. K. Chattopadhyay, B. Ghosh, F. A. Mautner, A. Frontera, D. Das, Inorg. Chem., 2013,**52**,13442.

108. T. C. Brunold, N. Tamura, N. Kitajima, Y. M. Oka, E. I. Solomon, J. Am. Chem. Soc., 1998,**120**,5674.

109. S. Hikichi, H. Komatsuzaki, N. Kitajima, M. Akita, M. Mukai, T. Kitagawa, Y. M. oka, Inorg. Chem., 1997,**36**,266.

110. Y. M. Oka, K. Fujisawa, N. Kitajima, Pure Appl. Chem., 1995,**67**,241.

111. M. K. Panda, M. M. Shaikh, R. J. Butcher, P. Ghosh, InorganicaChimicaActa., 2011,**372**,145.

112. Á. Kupán, J. Kaizer, G. Speier, M. Giorgi, M. Réglier, F.Pollreisz, J. Inorg. Biochem.,2009, **103**,389.

113. E. I. Solomon, P. Chen, M. Metz, S. K. Lee, A. E. Palner. Angew. Chem. Int. Ed., 2001,**40**,4570.

114. J. P. Klinman. Chem. Rev., 1996,**96**,2541.

115. M. R. Maurya, S.Agarwal, C. Bader, D.Rehder, Eur. J. Inorg. Chem. 2005, 147.

116. V. Conte, B. Floris, Inorg. Chim. Acta 2010,**363**,1935.

117. G. Zampella, P. Fantucci, V. L. Pecoraro, L. De Gioia, J. Am.Chem. Soc.,2005,**127**,953.

118. O. Bortolini, M. Carraro, V. Conte, S. Moro, J. Inorg. Biochem., 2000, **80**, 41.

119. J. Littlechild, E. G. Rodriguez, E. Coupe, A. Watts, M. Isupov, ACS Series Book, 2007,**974**,136.